

ADA 126670

ADP 300004

12

AD

CONTRACT REPORT ARBRL-CR-00510

NUMERICAL MODELING OF THE KINEMATICS  
OF TURBULENT MIXING IN HE-DRIVEN  
BLAST WAVES

Prepared by  
R & D Associates  
P. O. Box 9695  
Marina del Rey, CA 90291

DTIC  
ELECTE  
APR 1 1983

B

April 1983



**US ARMY ARMAMENT RESEARCH AND DEVELOPMENT COMMAND**  
**BALLISTIC RESEARCH LABORATORY**  
 ABERDEEN PROVING GROUND, MARYLAND

Approved for public release; distribution unlimited.

DTIC FILE COPY

Destroy this report when it is no longer needed.  
Do not return it to the originator.

Additional copies of this report may be obtained  
from the National Technical Information Service,  
U. S. Department of Commerce, Springfield, Virginia  
22161.

The findings in this report are not to be construed as  
an official Department of the Army position, unless  
so designated by other authorized documents.

*The use of trade names or manufacturers' names in this report  
does not constitute endorsement of any commercial product.*



UNCLASSIFIED

SECURITY CLASSIFICATION OF THIS PAGE(When Data Entered)

model does indeed generate turbulent mixing near the contact surface and nowhere else in the flow field. The magnitude of the turbulence depends on the turbulence model parameters, particularly the Rayleigh-Taylor coefficient,  $C_3$ , and the viscosity coefficient,  $C_4$ . Appropriate values for these parameters should be established by comparing the results of parametric calculations with experimental data.

UNCLASSIFIED

SECURITY CLASSIFICATION OF THIS PAGE(When Data Entered)



## LIST OF FIGURES

<u>Figure</u>		<u>Page</u>
1	Spatial distribution of the density field at various times (inviscid FCT calculation of a 1-lb spherical PBX-9404 charge detonated in air)	14
2	Spatial distribution of the momentum field at various times (inviscid FCT calculation of a 1-lb spherical PBX-9404 charge detonated in air)	15
3	Spatial distribution of the total energy field at various times (inviscid FCT calculation of a 1-lb spherical PBX-9404 charge detonated in air)	16
4	Spatial distribution of the velocity field at various times (inviscid FCT calculation of a 1-lb spherical PBX-9404 charge detonated in air)	17
5	Spatial distribution of the pressure field at various times (inviscid FCT calculation of a 1-lb spherical PBX-9404 charge detonated in air)	18
6	Spatial distribution of the internal energy field at various times (inviscid FCT calculation of a 1-lb spherical PBX-9404 charge detonated in air)	19
7	Spatial distribution of the species fraction field at various times (inviscid FCT calculation of a 1-lb spherical PBX-9404 charge detonated in air)	20
8	Spatial distribution of the effective gamma field at various times (inviscid FCT calculation of a 1-lb spherical PBX-9404 charge detonated in air)	21
9	Spatial distribution of the density field at various times (continuation of the FCT calculation of Figures 1-8 with the k-ε turbulence model activated)	23
10	Spatial distribution of the momentum field at various times (continuation of the FCT calculation of Figures 1-8 with the k-ε turbulence model activated)	24

LIST OF FIGURES (Cont.)

<u>Figure</u>		<u>Page</u>
11	Spatial distribution of the total energy field at various times (continuation of the FCT calculation of Figures 1-8 with the k- $\epsilon$ turbulence model activated)	25
12	Spatial distribution of the velocity field at various times (continuation of the FCT calculation of Figures 1-8 with the k- $\epsilon$ turbulence model activated)	26
13	Spatial distribution of the pressure field at various times (continuation of the FCT calculation of Figures 1-8 with the k- $\epsilon$ turbulence model activated)	27
14	Spatial distribution of the internal energy field at various times (continuation of the FCT calculation of Figures 1-8 with the k- $\epsilon$ turbulence model activated)	28
15	Spatial distribution of the species fraction field at various times (continuation of the FCT calculation of Figures 1-8 with the k- $\epsilon$ turbulence model activated)	29
16	Spatial distribution of the effective gamma field at various times (continuation of the FCT calculation of Figures 1-8 with the k- $\epsilon$ turbulence model activated)	30
17	Spatial distribution of the turbulent kinetic energy field at various times (continuation of the FCT calculation of Figures 1-8 with the k- $\epsilon$ turbulence model activated)	31
18	Spatial distribution of the turbulent kinetic energy dissipation rate at various times (continuation of the FCT calculation of Figures 1-8 with the k- $\epsilon$ turbulence model activated)	32
19	Spatial distribution of the total viscosity (laminar plus turbulent) field at various times (continuation of the FCT calculation of Figures 1-8 with the k- $\epsilon$ turbulence model activated)	33

## I. INTRODUCTION

Considered here is the theoretical modeling of turbulent mixing at density discontinuities in nonsteady compressible flows. It is well known that if a density discontinuity (or a strong density gradient) occurs in a pressure gradient of the opposite sign, then the flow field is hydrodynamically unstable in the Rayleigh-Taylor sense (Taylor, 1950).<sup>1</sup> Small perturbations occurring in such a region will amplify with time, and if the perturbations become large enough, they can lead to a local breakdown in the well-ordered flow; i.e., they can lead to turbulence.

One of the more interesting examples of density gradients working against pressure gradients to cause instabilities occurs in blast waves driven by solid high explosives (HE).<sup>\*</sup> After the detonation wave breaks out of the charge, the HE combustion gases expand to a high velocity ( $\sim 6$  km/s), pushing an air shock ahead. From one-dimensional inviscid calculations of this problem (Brode, 1957),<sup>2</sup> we know that a positive pressure gradient is formed throughout the flow field. Such calculations also indicate that there is a large density jump ( $\rho_{HE}/\rho_{air}$  can be as large as 70) across the contact surface. However, from high-speed photography of HE experiments, we know that this contact surface (which theoretically should be smooth) actually develops an irregular shape indicating the growth of instabilities. Evidence of mixing at the contact surface can be inferred from test results which show that the HE gases react with the shocked ambient gases and release

---

<sup>\*</sup> Similar gradients can occur in "shock-tube-type" flows driven by gases at very large initial densities.

1. Sir G. I. Taylor (1950), "Instability of Liquid Surfaces when Accelerated in a Direction Perpendicular to Their Plane," Proceedings of the Royal Society (London), A201, pp. 192-196.
2. H. L. Brode (1957), A Calculation of the Blast Wave from a Spherical Charge of TNT, Rand Corporation, RM-1965.

heat (i.e., afterburn) if the ambient gases contain oxygen (Matle, 1959, and Filler, 1956)<sup>3,4</sup>. Since this heat release can be of the same order as the energy released by the detonation wave (e.g., for TNT postdetonation energy release is about 2.5 times the detonation energy), it will affect the blast wave flow field and must be taken into account for accurate numerical simulations of such flows.

This report describes the numerical work that RDA has performed to simulate the kinematics\* of the turbulent mixing associated with such HE-driven blast waves. A k-ε turbulence model was programmed and combined with RDA's minimal-diffusion Flux-Corrected Transport (FCT) module which solves the gas dynamic conservation laws on a sliding grid. Source terms were included in the k-ε equations to model the above-described Rayleigh-Taylor mechanism to generate turbulence. The governing equations are described in Section II. Preliminary numerical studies (as described in Section III) indicate that this model does, indeed, generate turbulent kinetic energy at the HE/air interface of HE-driven blast waves. Conclusions and recommendations are offered in Section IV.

---

\* Energetics (i.e., heat release) was neglected for the preliminary work.

3. C. C. Matle (1959), The Contribution of Afterburning to the Air Blast from Explosives, NAVORD Report 6234.
4. W. S. Filler (1956), "Post-Detonation Pressure and Thermal Studies of Solid Explosives in a Closed Chamber," Sixth (Int) Symposium on Combustion, pp. 648-657.

## II. FORMULATION

The time evolution of the mean flow is governed by the conservation of mass, momentum and energy which may be written as follows for point ( $j=2$ ), line ( $j=1$ ), or plane ( $j=0$ ) symmetric flow:

$$\frac{\partial}{\partial t} \rho + \frac{1}{r^j} \frac{\partial}{\partial r} (r^j \rho u) = 0 \quad (1)$$

$$\frac{\partial}{\partial t} (\rho u) + \frac{1}{r^j} \frac{\partial}{\partial r} (r^j \rho u^2) = -\frac{\partial}{\partial r} (p + \frac{2}{3} \rho k) \quad (2)$$

$$\begin{aligned} \frac{\partial}{\partial t} (\rho E) + \frac{1}{r^j} \frac{\partial}{\partial r} (r^j \rho u E) = & -\frac{1}{r^j} \frac{\partial}{\partial r} r^j u (p + \frac{2}{3} \rho k) \\ & + \frac{1}{r^j} \frac{\partial}{\partial r} r^j \mu_T \left( \frac{1}{\sigma_{t,h}} \frac{\partial h}{\partial r} + \frac{1}{\sigma_{t,k}} \frac{\partial k}{\partial r} \right) + \dot{Q} \end{aligned} \quad (3)$$

where mass-averaged properties of the mixture are

- $\rho$  = density
- $u$  = velocity
- $E$  = total energy =  $e + \frac{1}{2} u^2 + k$
- $e$  = internal energy
- $p$  = pressure
- $\dot{Q}$  = rate of energy release per unit volume
- $h$  = enthalpy

and the turbulence parameters are

- $k$  = turbulence kinetic energy per unit mass
- $\sigma_{T,\beta}$  = turbulent Prandtl number for the variable  $\beta$
- $\mu_T$  = total viscosity =  $\mu_f + C_\mu \rho k^2/\epsilon$
- $\mu_f$  = molecular viscosity

For a mixture of  $N$  component gases, one must solve  $N-1$  species transport equations in addition to the mass conservation law for the mixture (Eq. 1). The species transport equations have the form

$$\frac{\partial}{\partial t} \rho f_a + \frac{1}{r^j} \frac{\partial}{\partial r} (r^j \rho f_a u) = \frac{1}{r^j} \frac{\partial}{\partial r} \left( r^j \frac{\mu_T}{\sigma_{t,f}} \frac{\partial f_a}{\partial r} \right) + \dot{S}_a \quad (4)$$

where  $f_\alpha$  = mass-averaged, mass fraction of component  $\alpha$   
 $= \rho_\alpha / \rho$  (while  $\sum_\alpha f_\alpha = 1$ )

$\dot{S}_\alpha$  = rate of creation of component  $\alpha$  (with  $\sum_\alpha \dot{S}_\alpha = 0$ )

As shown by Issa (1980),<sup>5</sup> a one-dimensional k- $\epsilon$  turbulence model can be used to simulate turbulent mixing driven by the Rayleigh-Taylor mechanism. The transport equations for the turbulence kinetic energy, k, and the turbulence kinetic energy dissipation rate,  $\epsilon$ , acquire the following form:

$$\frac{\partial}{\partial t} (\rho k) + \frac{1}{r^j} \frac{\partial}{\partial r} (r^j \rho k u) = \frac{1}{r^j} \frac{\partial}{\partial r} \left( r^j \frac{\nu_t}{\sigma_{t,k}} \frac{\partial k}{\partial r} \right) + G - \rho \epsilon \quad (5)$$

$$\frac{\partial}{\partial t} (\rho \epsilon) + \frac{1}{r^j} \frac{\partial}{\partial r} (r^j \rho \epsilon u) = \frac{1}{r^j} \frac{\partial}{\partial r} \left( r^j \frac{\nu_t}{\sigma_{t,\epsilon}} \frac{\partial \epsilon}{\partial r} \right) + C_1 G / k - C_2 \rho \epsilon^2 / k \quad (6)$$

where

$$G = -\frac{2}{3} \frac{k}{r^j} \frac{\partial}{\partial r} (r^j u) - C_3 \frac{\nu_t}{\rho} \frac{\partial \rho}{\partial r} \frac{\partial p}{\partial r} \quad (7)$$

Here G represents a source/sink for turbulence kinetic energy. The first term in G is proportional to the flow divergence and tends to kill turbulence in expanding flows. The second term is proportional to the product of the mean pressure and density gradients. When these gradients have opposite signs, then G can become positive. As will be shown, the pressure and density gradients do have such opposite signs near the contact surface of an HE-driven blast wave and turbulence indeed grows there. In other regions of the flow (e.g., at the shocks and in the rarefaction wave), the pressure and density gradients have similar signs and turbulence is suppressed.

5. R. I. Issa (1980), Modeling of Turbulent Mixing at Density Discontinuities in Nonsteady Compressible Flows, R & D Associates. RDA-TR-107605-001.

### III. NUMERICAL STUDIES

The k-ε turbulence equations described in the previous section were programmed on the computer and incorporated into the one-dimensional hydrocode, RDAFCT. This code uses the FCT module labeled JPBFACT<sup>6</sup> to solve general conservation laws on a sliding grid:

$$\frac{\partial}{\partial t} \int_{\delta A(t)} \underline{w} dA = - \oint_{\delta A(t)} \underline{w} (\vec{u} - \vec{u}_g) \cdot dA + \oint_{\delta A(t)} \tau dA \quad (8)$$

where  $\underline{w} = (\rho, \rho \vec{u}, \rho E, \rho f, \text{etc.})$  and the grid motion satisfies  $dA(t) = \underline{u}_g(t) dA(t)$ . The module is called successively for each conservation equation (i.e., Eqs. (1) to (6)) to advance the flow field one time step. NRL's newest transport, diffusion and antidiffusion coefficients are employed to give sixth-order phase and fourth-order amplitude properties for the numerical algorithm.

a. Initial conditions--As a test problem, we chose to simulate the evolution of the flow field associated with the detonation of a 1-lb spherical charge of PBX-9404 in air. Predetonation conditions for the charge were

$$R_C = 1.88973 \text{ cm}$$

$$\rho_C = 1.84 \text{ g/cm}^3$$

while the ambient air conditions were taken as

$$P_a = 1.01325 \times 10^6 \text{ dy/cm}^2$$

$$\rho_a = 1.225 \times 10^{-3} \text{ g/cm}^3$$

$$T_a = 288.4^\circ \text{K}$$

It was assumed that the charge was center-detonated. Initial conditions for the numerical calculations were taken at the instant the detonation wave reached the charge radius. It was assumed that the flow field corresponded to that of an ideal, Chapman-Jouquet (CJ) detonation wave; this field was obtained from subroutine CJDET which provides the similarity solution for any given explosive (Kuhl, 1978).<sup>7</sup>

6. J. P. Boris (1976), Flux-Corrected Transport Modules for Solving Generalized Continuity Equations, Naval Research Laboratory, Memorandum Report 3237.

7. A. L. Kuhl, M. R. Seizew (1978), Analysis of Ideal, Strong, Chapman-Jouquet Detonations, TRW Report 78.4735.9-13.

b. Equation-of-state--The detonation products were modeled by the Jones-Wilkins-Lee (JWL) equation-of-state (Dobratz, 1974)<sup>8</sup> which provides the pressure as a function of density and internal energy in the form

$$p(\rho, e) = A \left( 1 - \frac{\omega \rho}{R_1 \rho_0} \right) \exp(-R_1 \rho_0 / \rho) + B \left( 1 - \frac{\omega \rho}{R_2 \rho_0} \right) \exp(-R_2 \rho_0 / \rho) + \omega p e \quad (9)$$

The JWL parameters for PBX-9404 are

$$\begin{aligned} A &= 8.545 \text{ Mbars} \\ B &= 0.20493 \text{ Mbars} \\ R_1 &= 4.60 \\ R_2 &= 1.35 \\ \omega &= \gamma - 1 = 0.25 \end{aligned}$$

while the CJ detonation parameters for this explosive are

$$\begin{aligned} p_{CJ} &= \rho_0 w_{CJ}^2 / (\Gamma + 1) = 370 \text{ kbars} \\ \rho_{CJ} &= \rho_0 (\Gamma + 1) / \Gamma = 2.485 \text{ g/cm}^3 \\ w_{CJ} &= 8.8 \text{ km/s} \\ u_{CJ} &= w_{CJ} / (\Gamma + 1) = 2.28 \text{ km/s} \\ q_{CJ} &= E_0 / \rho_0 = 5.543 \times 10^{10} \text{ erg/g} \\ \Gamma_{CJ} &= 2.85 \\ e_{CJ} &= q_{CJ} + 1/2 u_{CJ}^2 = 8.142 \times 10^{10} \text{ erg/g} \end{aligned}$$

Local thermodynamic equilibrium was assumed for the air. The pressure was related to the density and internal energy by an effective gamma:

$$p = (\gamma_e - 1) \rho e \quad (10)$$

where  $\gamma_e = \gamma_e(\rho, e)$  was obtained from a table-lookup subroutine which uses Gilmore's data for real air (Gilmore, 1955).<sup>9</sup> Two gas species were considered: air and detonation products. Computational cells containing air were initialized with  $f=0$ , while cells containing detonation products were initialized with  $f=1$ . A transport equation was then included for the species fraction  $f$ . In the present nonreactive case,  $f$  served

8. B. Dobratz (1974), Properties of Chemical Explosives and Explosive Simulants, Lawrence Livermore Laboratory Report UCRL-51319 Rev. 1.

9. F. R. Gilmore (1955), Equilibrium Composition and Thermodynamic Properties of Air to 24000°K, Rand Report RM-1543.

simply as a flag to discriminate which cells contained air and which cells contained HE. Pressures in mixed cells (where  $0.1 < f < 0.9$ ) were blended according to Dalton's law. For the present study, heat release due to turbulent mixing near the HE/air interface was neglected ( $\dot{S}_q = 0$ ).

c. Results--As a baseline, we first performed an inviscid calculation of this HE-driven blast wave (i.e.,  $k = \epsilon = \mu_T = 0$ ). We found it necessary to use very fine zoning for this problem. The grid spacing was initialized as one tenth of one percent of the shock radius ( $\Delta/R_S = .001$ ) in the outer region of the charge ( $0.08 < r/R_S < 1.0$ ) yielding 200 cells, and then allowed to increase according to an interest rate formula ( $0 < r/R_S < 0.8$ ) over 50 cells, with a grand total of 250 cells inside the charge. The cell containing the primary or outer shock front was moved with a velocity about equal to the instantaneous shock velocity,  $w_S$ , so that this shock remained approximately fixed in the grid. Cell interfaces inside the shock were assigned velocities linearly proportional to the radius:

$$(u_g)_{i+k} = w_S \cdot r_{i+k} / R_S \quad (11)$$

Note that this grid law produces a linear dilation of the grid, and hence preserves the initial mesh space distribution--a very useful attribute for this case. It keeps the cells packed where all the action is--near the contact surface and shock front!

Figures 1-8 show the inviscid flow field spatial distributions as calculated for this HE-driven blast wave at various instants in time, starting from the CJ detonation flow field (cycle 0) out at a point in time where the air shock has reached about two charge radii (cycle 800). Included near the bottom of each figure is the mesh distribution for the last displayed time. Note in particular the density distributions of Figure 1 which show a primary shock (S1), followed by a contact surface (CS), and then a secondary shock (S2). The latter is an inward-facing shock that is being swept outward by the supersonic flow. At later times, this secondary shock starts to move inward and eventually implodes.

Next, a turbulence calculation was performed. Initial conditions were taken as the flow field at the end on the aforementioned inviscid calculation for the following reasons:

- At this point the three discontinuities had separated from each other and were well resolved on the mesh.
- This allowed an accurate calculation of the pressure and density gradients which fed into the turbulence source term, G.

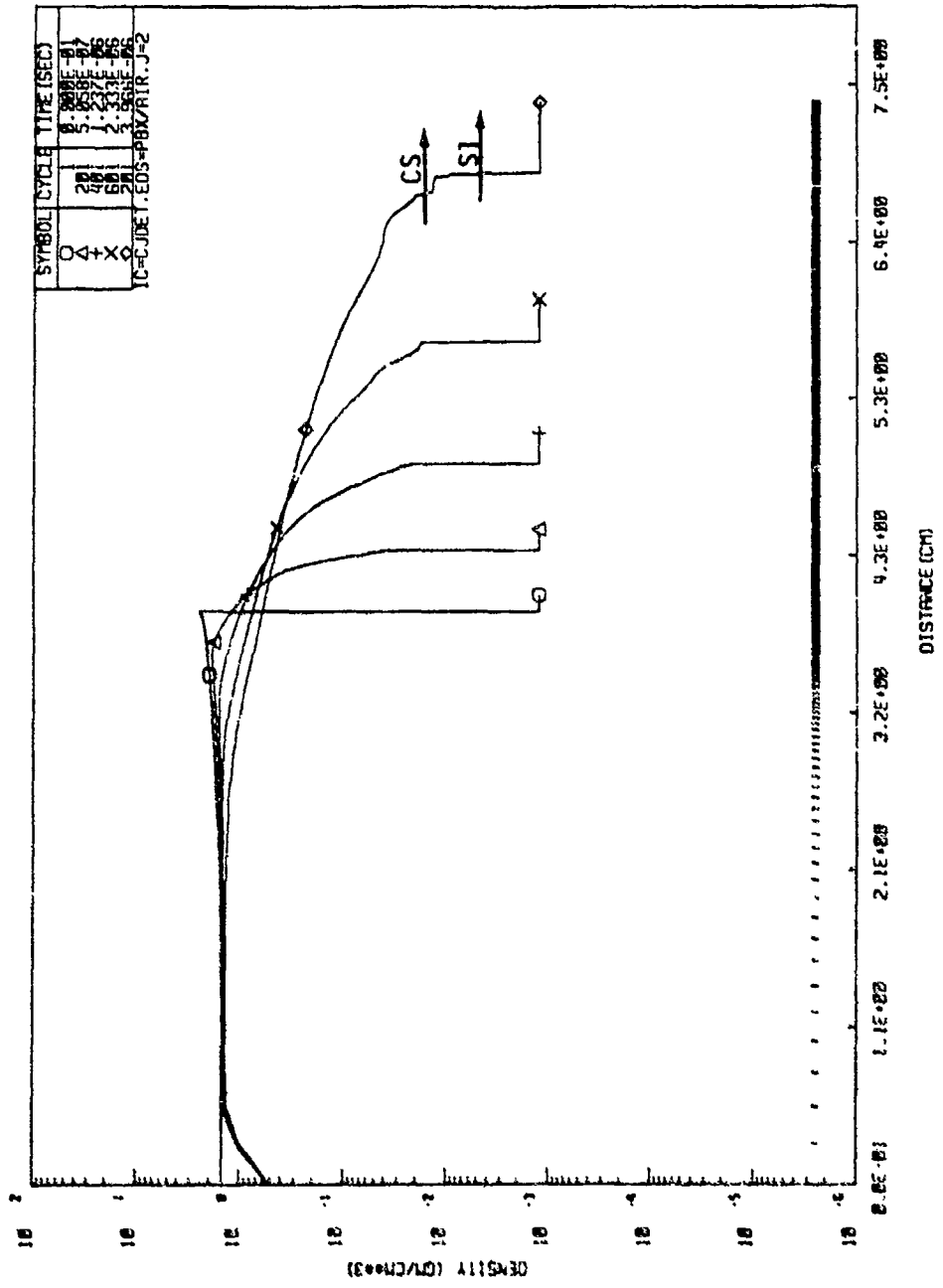


Figure 1. Spatial distribution of the density field at various times (inviscid FCT calculation of a 1-lb spherical PBX-9404 charge detonated in air).

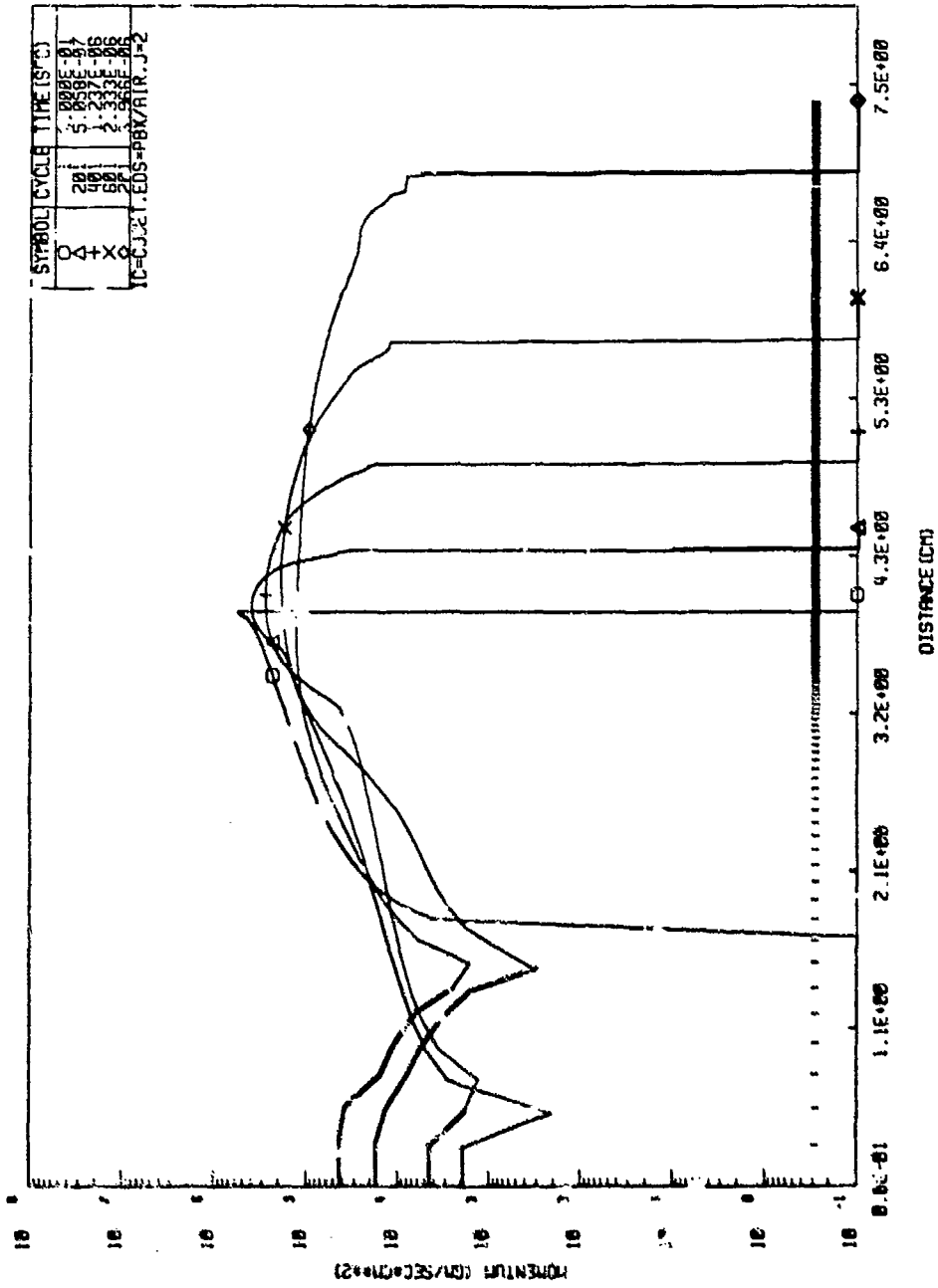


Figure 2. Spatial distribution of the momentum field at various times (inviscid FCT calculation of a 1-lb spherical PBX-9404 charge detonated in air).

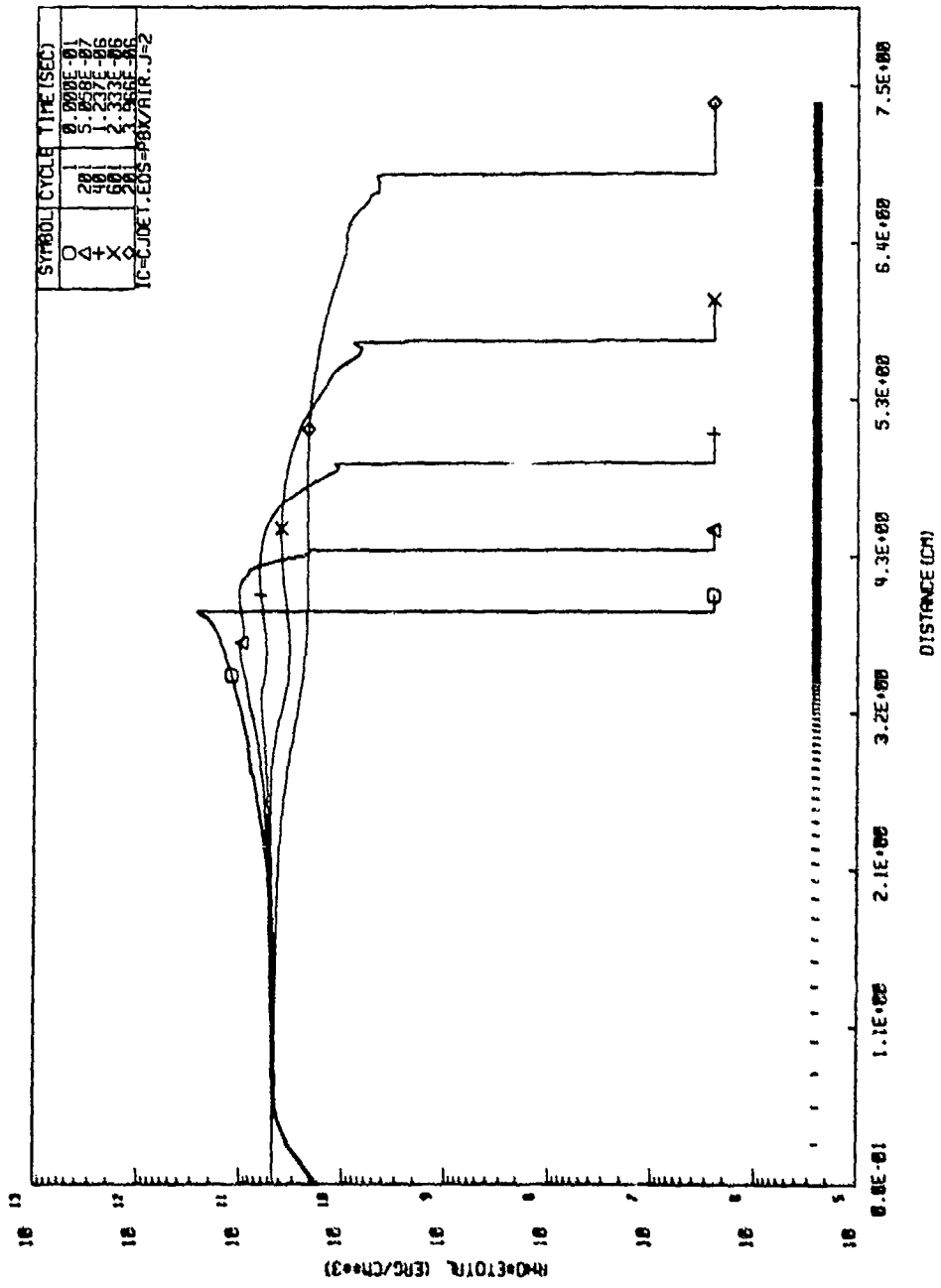


Figure 3. Spatial distribution of the total energy field at various times (inviscid FCT calculation of a 1-lb spherical PBX-9404 charge detonated in air).

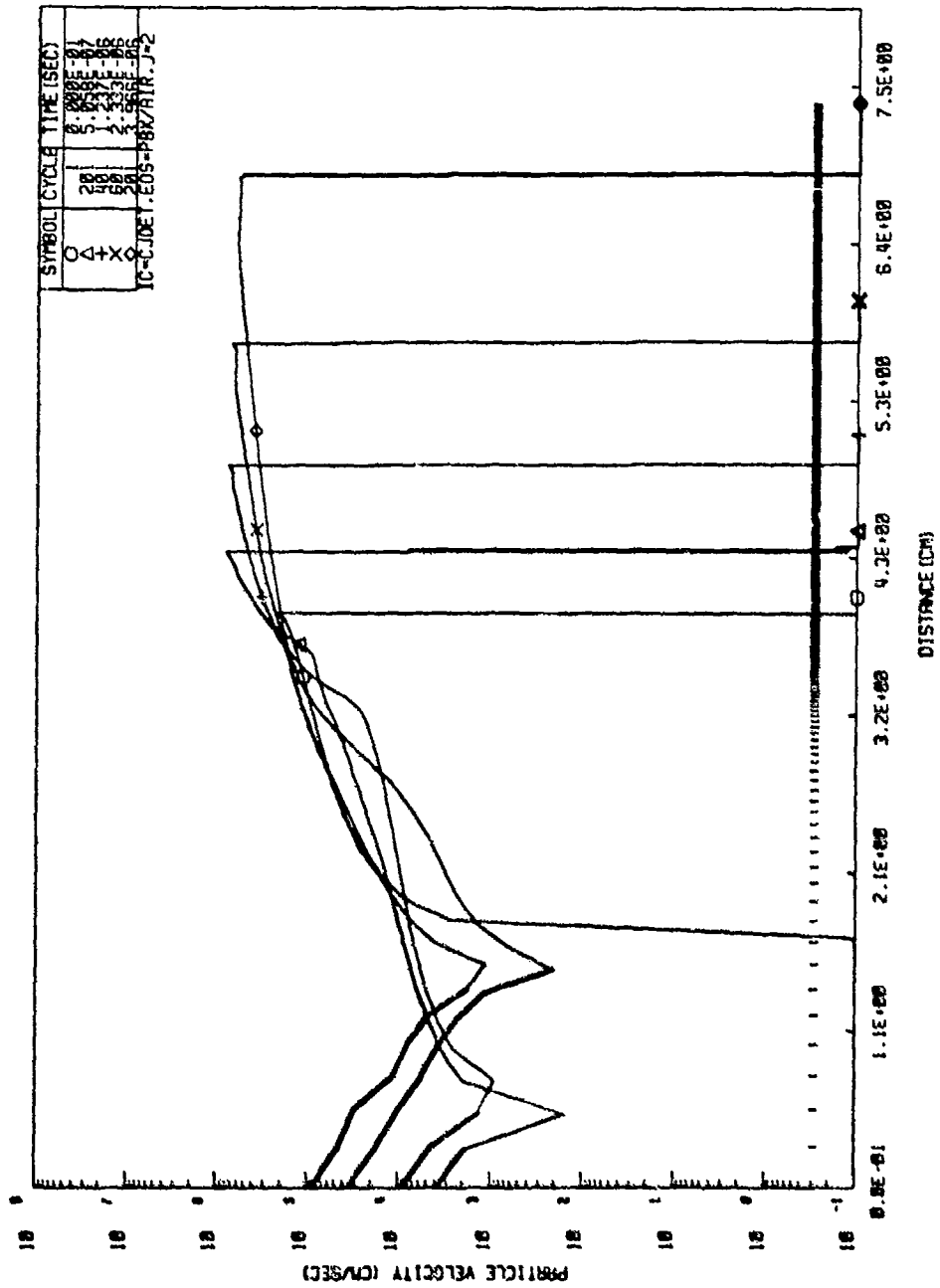


Figure 4. Spatial distribution of the velocity field at various times (inviscid FCT calculation of a 1-lb spherical PBX-9404 charge detonated in air).

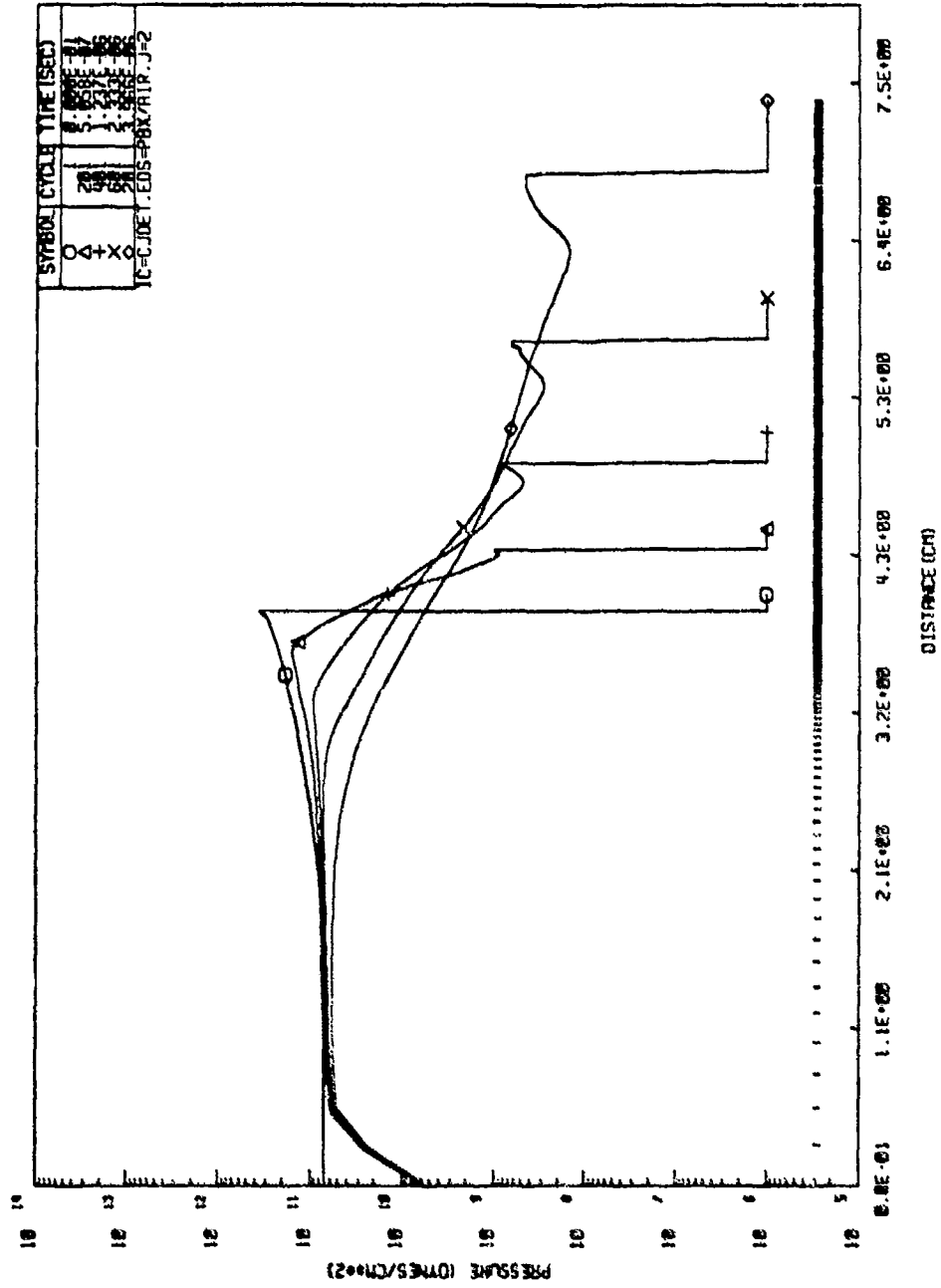


Figure 5. Spatial distribution of the pressure field at various times (inviscid FCT calculation of a 1-lb spherical PBX-9404 charge detonated in air).

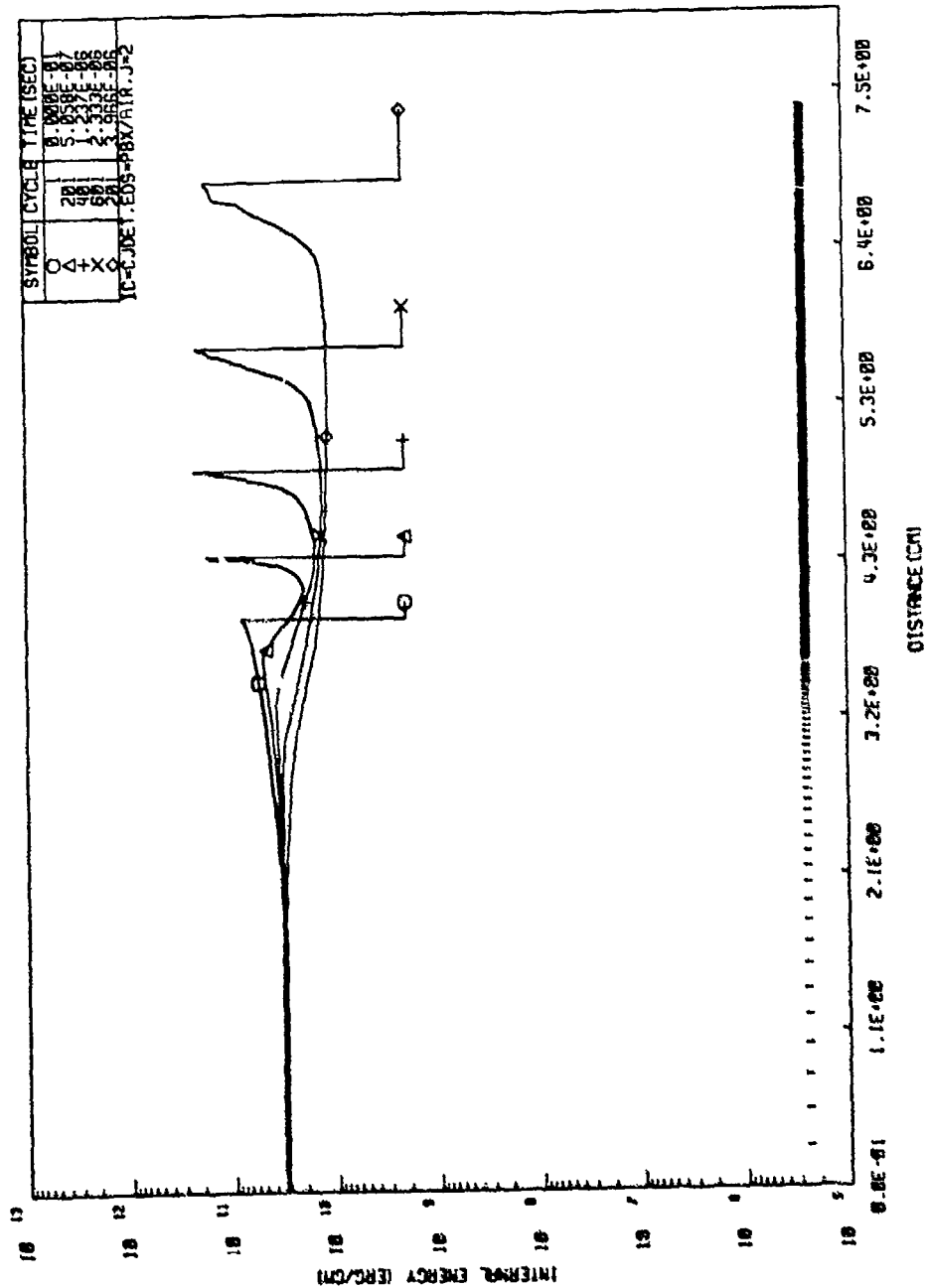


Figure 6. Spatial distribution of the internal energy field at various times (inviscid PCT calculation of a 1-lb spherical PBX-9404 charge detonated in air).

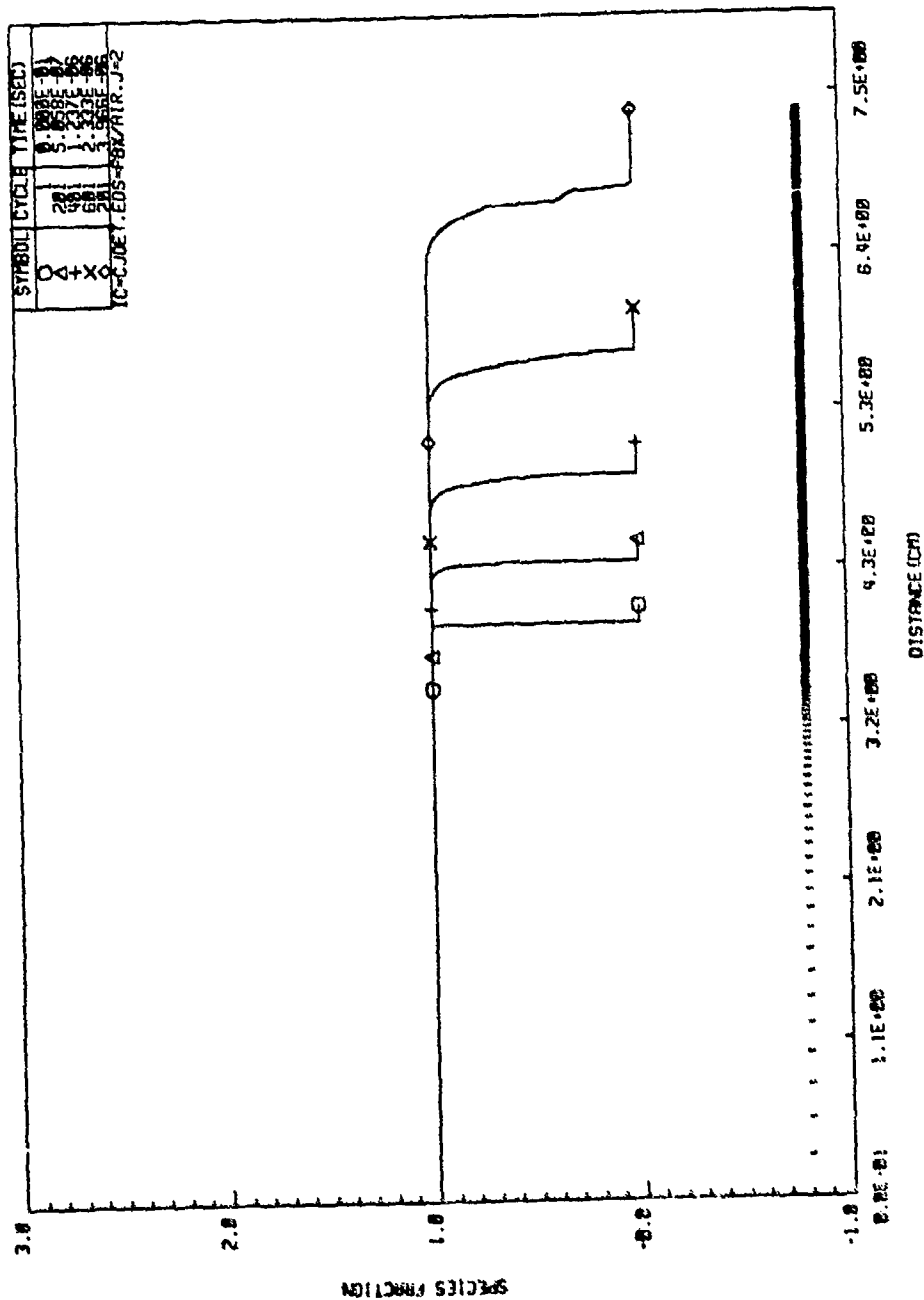


Figure 7. Spatial distribution of the species fraction field at various times (inviscid PCT calculation of a 1-lb spherical PBX-9404 charge detonated in air).

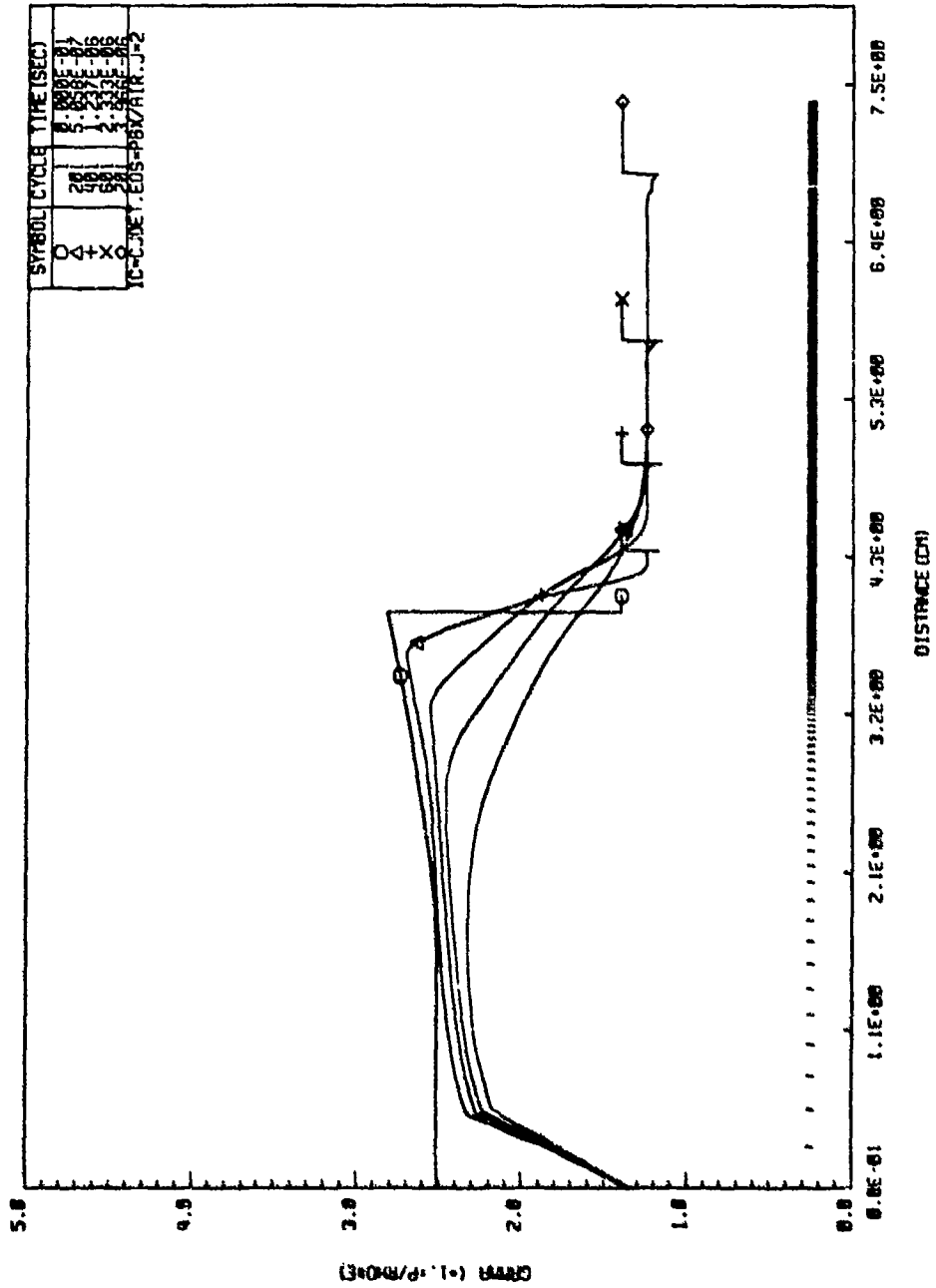


Figure 6. Spatial distribution of the effective gamma field at various times (inviscid PCT calculation of a 1-lb spherical PBX-9404 charge detonated in air).

The values of the k- $\epsilon$  model parameters were taken as those established from turbulent shear flow

$$\begin{aligned}C_1 &= 1.44 \\C_2 &= 1.92 \\ \sigma_{T,\beta} &= 1.0 \text{ for } \beta = h, k, f \\ \sigma_{T,\epsilon} &= 1.3\end{aligned}$$

while the viscosity coefficient,  $C_\mu$ , and the Rayleigh-Taylor coefficient,  $C_3$ , were assumed to be:

$$\begin{aligned}C_\mu &= 0.009 \\C_3 &= 1.0\end{aligned}$$

Figures 9 through 19 give the evolution of the flow field at 100 and 200 cycles after the turbulence terms were turned on. These figures show a narrow region of the flow field in the vicinity of the contact surface. Consider in particular Figures 17, 18 and 19 which depict the calculated turbulent kinetic energy,  $k$ , dissipation rate,  $\epsilon$ , and total viscosity,  $\mu_T$ . Comparing these parameters with the density distribution shows that the turbulent kinetic energy grows rapidly in the vicinity of the contact surface and nowhere else. After 200 cycles,  $k \sim 5 \times 10^8$  erg/g while internal and kinetic energies are greater than  $10^{10}$  erg/g. Note that the dissipation rate is also growing; hence, the evolution of the turbulence kinetic energy will depend on the delicate balance between the generation terms and the decay terms. These, in turn, depend on the particular values chosen for  $C_3$  and  $C_\mu$ . A detailed investigation of these effects is an appropriate subject for future studies.

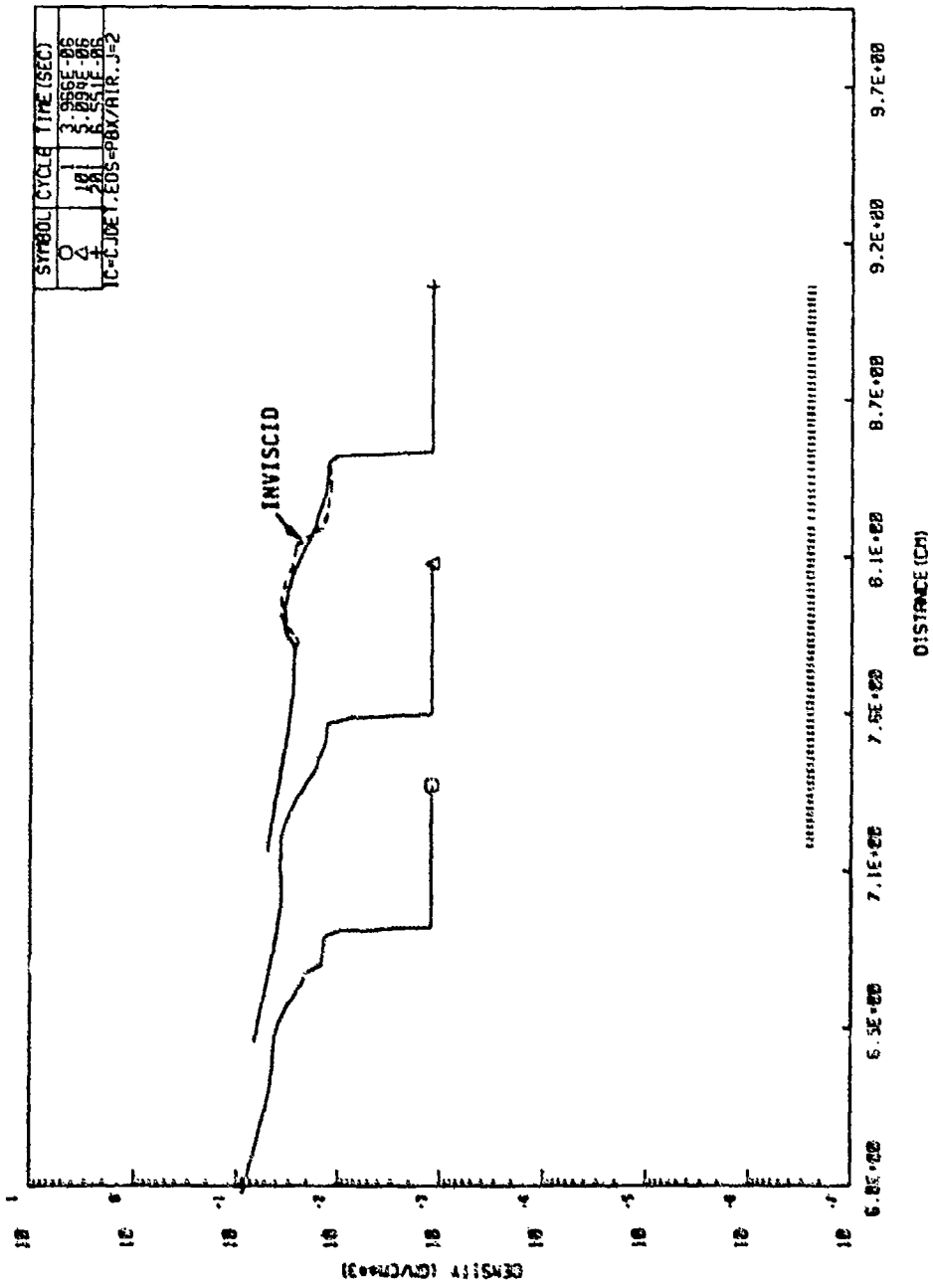


Figure 9. Spatial distribution of the density field at various times (continuation of the PCT calculation of Figures 1-8 with the k-ε turbulence model activated).

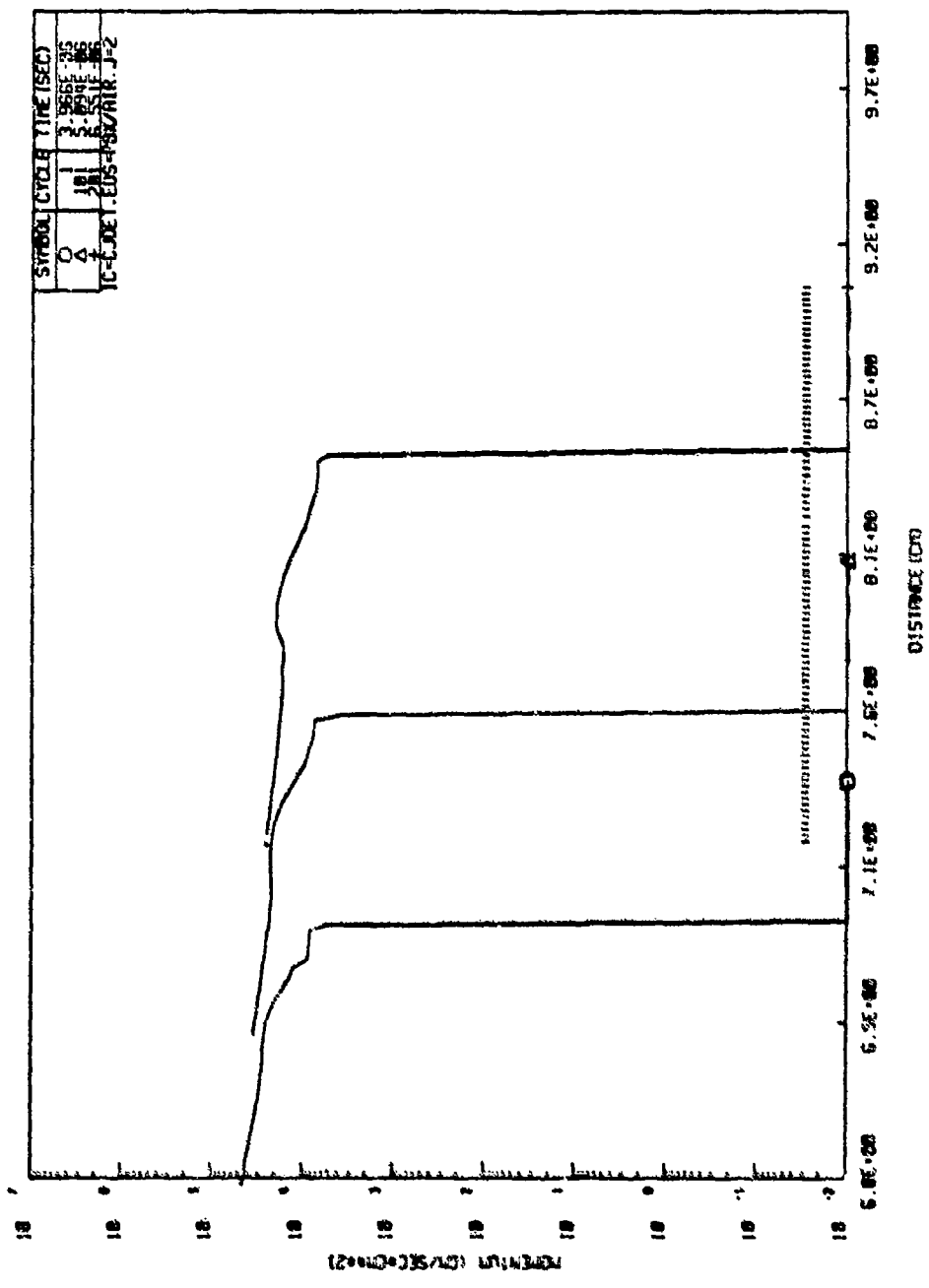


Figure 10. Spatial distribution of the momentum field at various times (continuation of the FCT calculation of Figures 1-8 with the k-ε turbulence model activated).

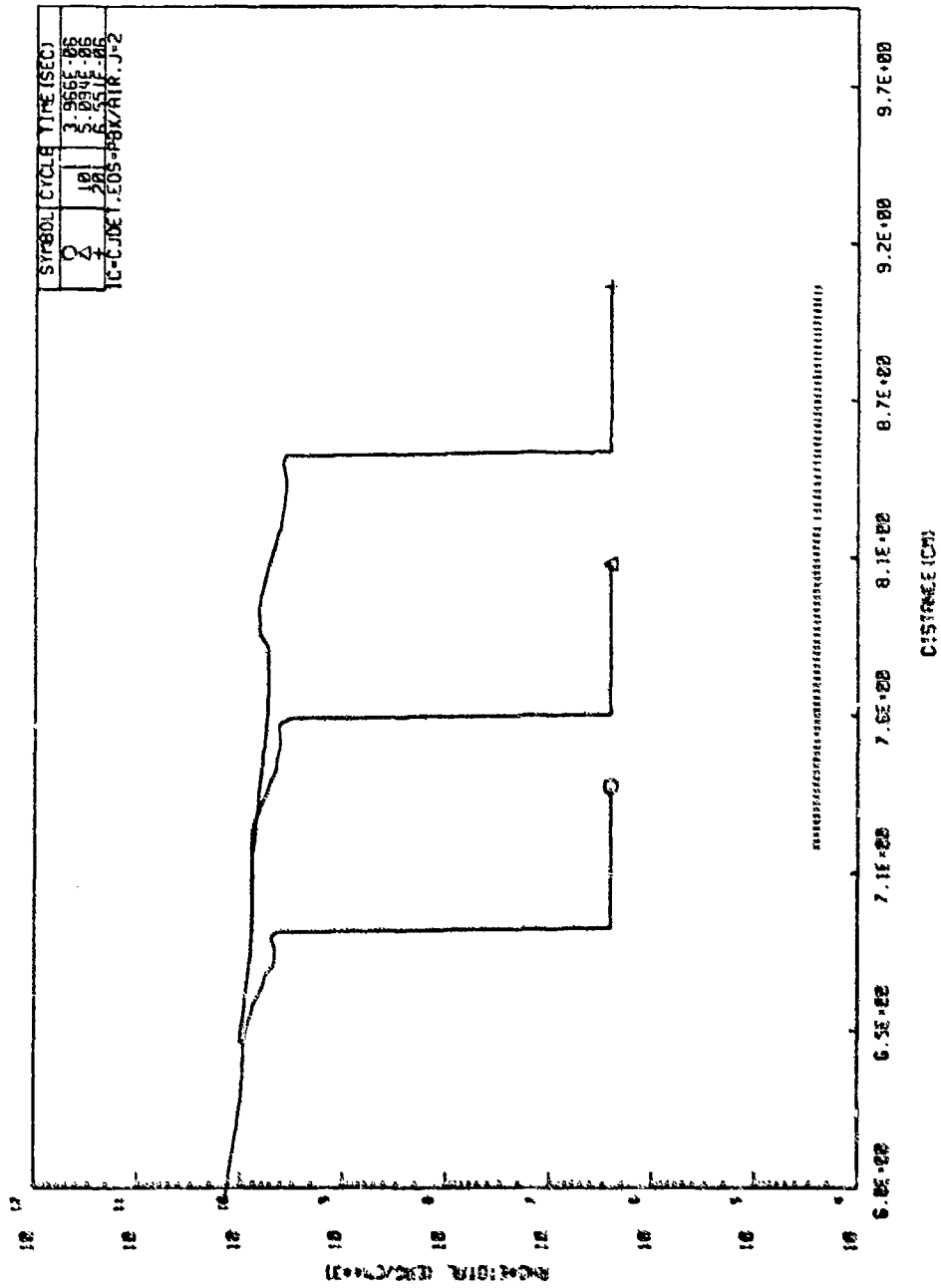


Figure 11. Spatial distribution of the total energy field at various times (continuation of the FCT calculation of Figures 1-8 with the k-ε turbulence model activated).

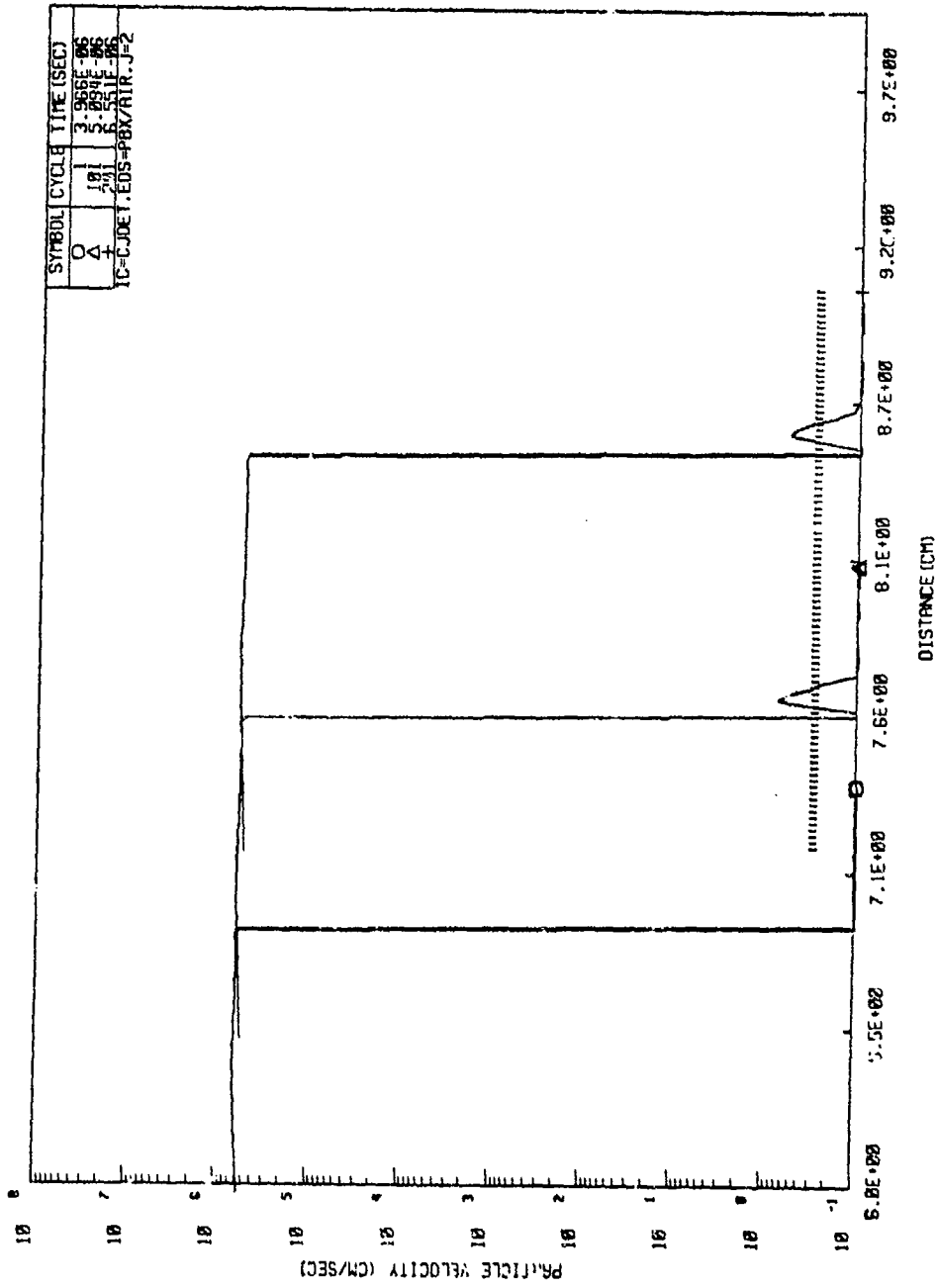


Figure 12. Spatial distribution of the velocity field at various times (continuation of the FCT calculation of Figures 1-8 with the k-ε turbulence model activated).

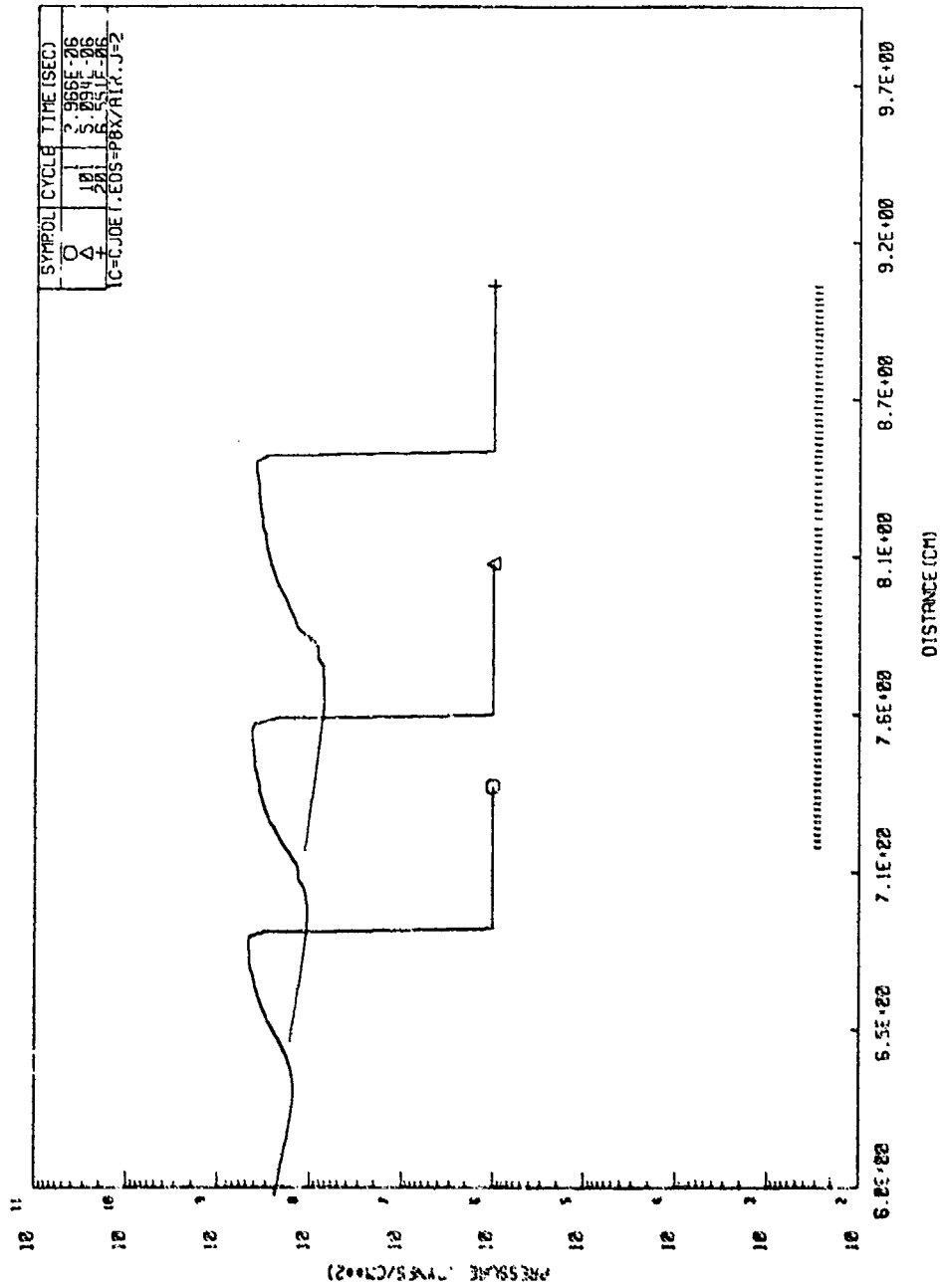


Figure 13. Spatial distribution of the pressure field at various times (continuation of the FCT calculation of Figures 1-8 with the k-ε turbulence model activated).

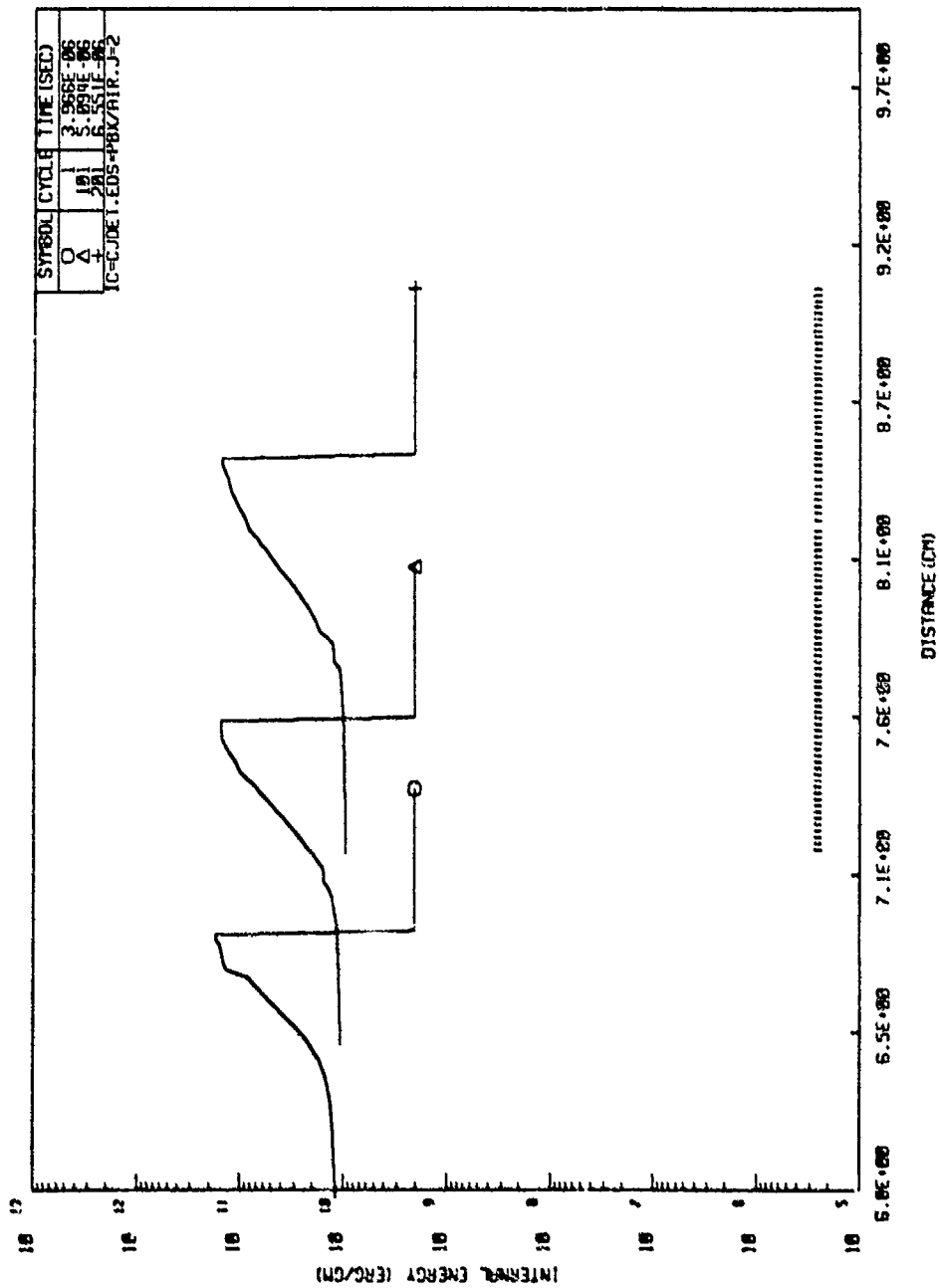


Figure 14. Spatial distribution of the internal energy field at various times (continuation of the FCT calculation of Figures 1-8 with the  $k-\epsilon$  turbulence model activated).

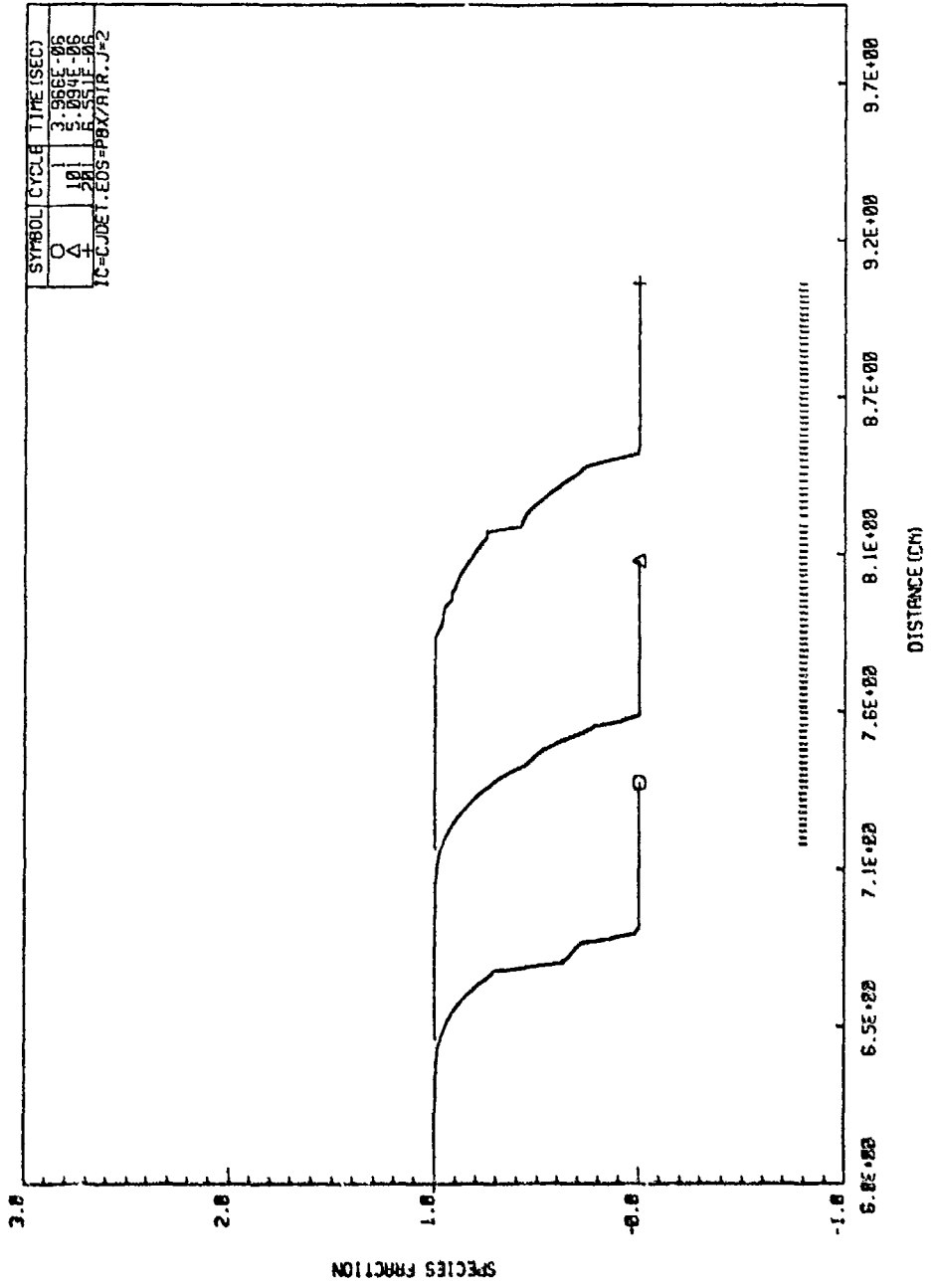


Figure 15. Spatial distribution of the species fraction field at various times (continuation of the FCR calculation of Figures 1-8 with the k-ε turbulence model activated).

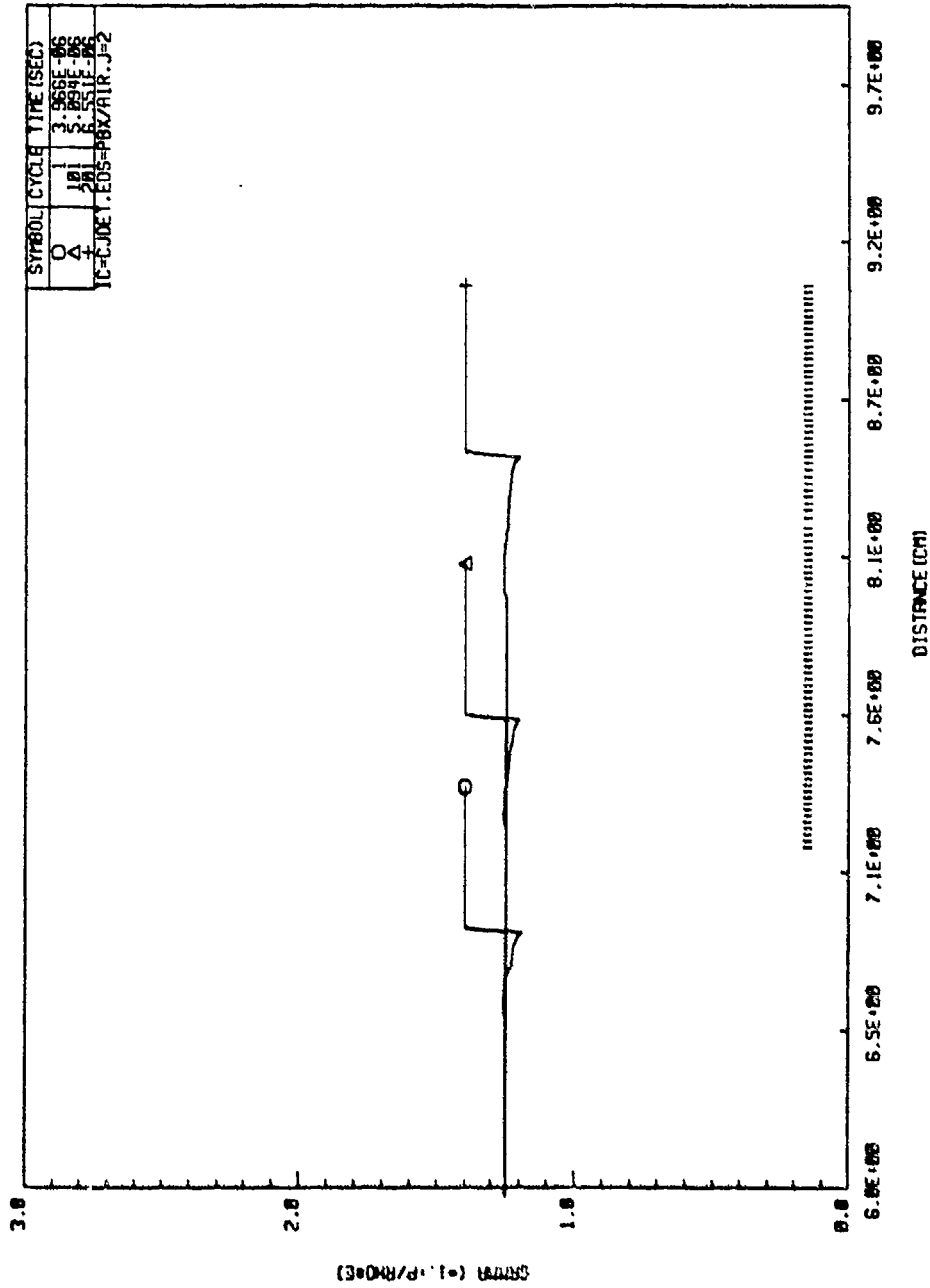


Figure 16. Spatial distribution of the effective gamma field at various times (continuation of the FCT calculation of Figures 1-8 with the k-ε turbulence model activated).

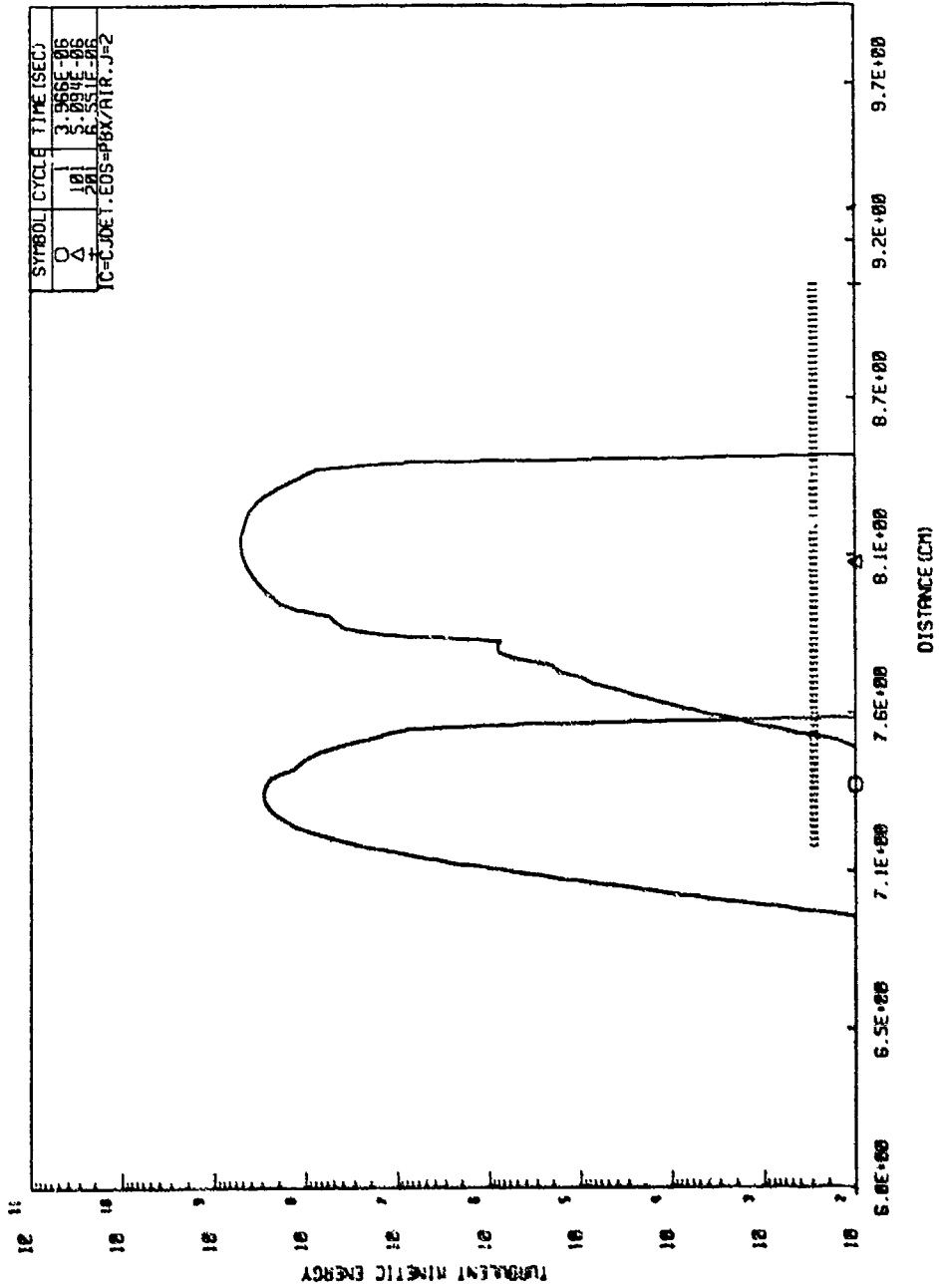


Figure 17. Spatial distribution of the turbulent kinetic energy field at various times (continuation of the FCT calculation of Figures 1-8 with the k-ε turbulence model activated).

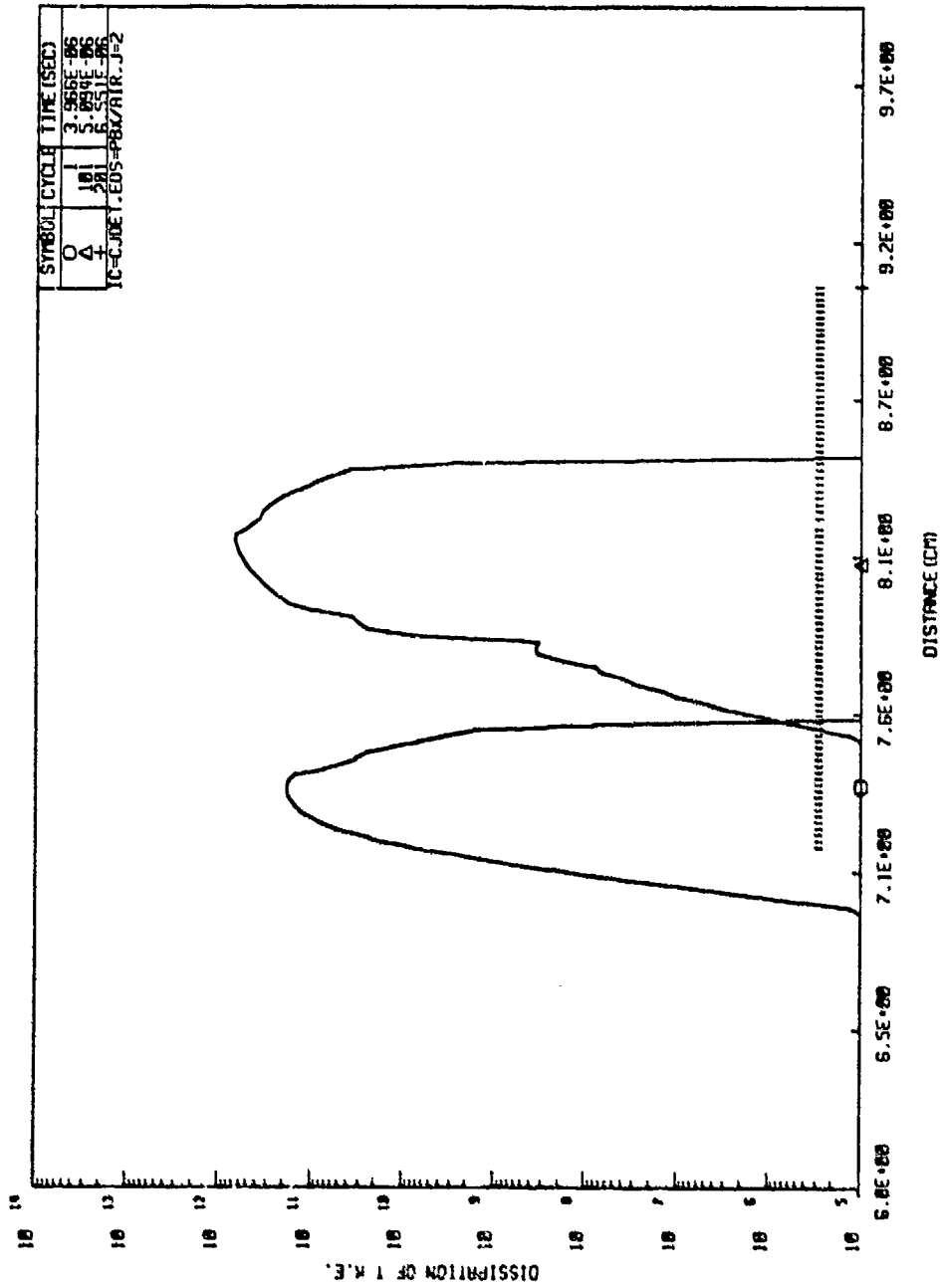


Figure 18. Spatial distribution of the turbulent kinetic energy dissipation rate at various times (continuation of the FCT calculation of Figures 1-8 with the k-ε turbulence model activated).

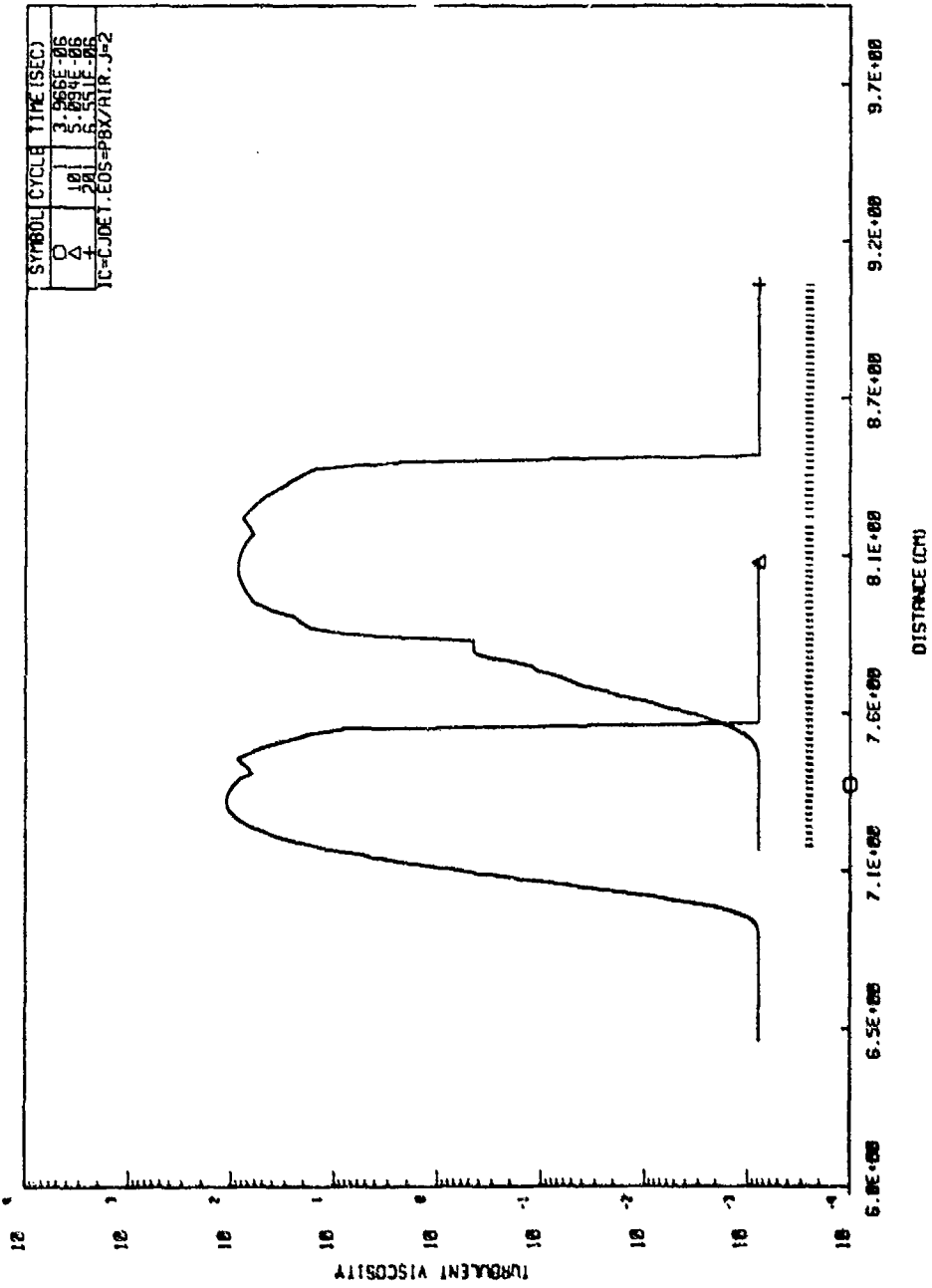


Figure 19. Spatial distribution of the total viscosity (laminar plus turbulent) field at various times (continuation of the FCT calculation of Figures 1-8 with the k-ε turbulence model activated).

#### IV. CONCLUSIONS AND RECOMMENDATIONS

We have shown here that the present  $k$ - $\epsilon$  turbulence model does indeed predict the rapid growth of turbulence in the vicinity of the contact surface for HE-driven blast waves. Parametric studies should be performed with this model to pin down the constants, especially  $C_3$  and  $C_\mu$ . Such kinematic calculations should be verified with experimental data. In addition, a heat release model should be formulated and incorporated into the hydrocode. Calculations including such energetics (i.e., afterburning) should then be performed for explosives which afterburn more strongly (e.g., TNT and Pentolite) and more weakly (e.g., PBX-9404), and such calculations should then be compared with appropriate experimental data (pressure records, photography and thermal radiation measurements of the fireball) and inviscid calculations to determine the importance of afterburning for various types of explosives.

## REFERENCES

1. Sir G. I. Taylor (1950), "Instability of Liquid Surfaces when Accelerated in a Direction Perpendicular to Their Plane," Proceedings of the Royal Society (London), A201, pp. 192-196.
2. H. L. Brode (1957), A Calculation of the Blast Wave from a Spherical Charge of TNT, Rand Corporation, RM-1965.
3. C. C. Matle (1959), The Contribution of Afterburning to the Air Blast from Explosives, NAVORD Report 6234.
4. W. S. Filler (1956), "Post-Detonation Pressure and Thermal Studies of Solid Explosives in a Closed Chamber," Sixth (Int) Symposium on Combustion, pp. 648-657.
5. R. I. Issa (1980), Modeling of Turbulent Mixing at Density Discontinuities in Nonsteady Compressible Flows, R & D Associates, RDA-TR-107605-001.
6. J. P. Boris (1976), Flux-Corrected Transport Modules for Solving Generalized Continuity Equations, Naval Research Laboratory, Memorandum Report 3237.
7. A. L. Kuhl, M. R. Seizew (1978), Analysis of Ideal, Strong, Chapman-Jouquet Detonations, TRW Report 78.4735.9-13.
8. B. Dobratz (1974), Properties of Chemical Explosives and Explosive Simulants, Lawrence Livermore Laboratory Report UCRL-51319 Rev. 1.
9. F. R. Gilmore (1955), Equilibrium Composition and Thermodynamic Properties of Air to 24000°K, Rand Report RM-1543.

DISTRIBUTION LIST

<u>No. of Copies</u>	<u>Organization</u>	<u>No. of Copies</u>	<u>Organization</u>
12	Administrator Defense Technical Info Center ATTN: DTIC-DDA Cameron Station Alexandria, VA 22314	1	Director Defense Communications Agency ATTN: 930 Washington, DC 20305
1	Director of Defense Research & Engineering ATTN: DD/TWP Washington, DC 20301	9	Director Defense Nuclear Agency ATTN: DDST TIPL/Tech Lib SPSS/K. Goering G. Ullrich SPTD/T. Kennedy SPAS STSP NATD NATA Washington, DC 20305
1	Asst. to the Secretary of Defense (Atomic Energy) ATTN: Document Control Washington, DC 20301		
1	Director Defense Advanced Research Projects Agency ATTN: Tech Lib 1400 Wilson Boulevard Arlington, VA 22209	2	Commander Field Command, DNA ATTN: FCPR FCTMOF Kirtland AFB, NM 87115
2	Director Federal Emergency Management Agency ATTN: Mr. George Sisson/RF-SR Technical Library Washington, DC 20301	1	Commander Field Command, DNA Livermore Branch ATTN: FCPR P.O. Box 808 Livermore, CA 94550
1	Director Defense Intelligence Agency ATTN: DT-2/Wpns & Sys Div Washington, DC 20301	1	Director Inst for Defense Analyses ATTN: Library 1801 Beauregard St. Alexandria, VA 22311
1	Director National Security Agency ATTN: E. F. Butala, R15 Ft. George G. Meade, MD 20755	1	Director US Army BMD Program Office ATTN: John Shea 5001 Eisenhower Avenue Alexandria, VA 22333
1	Director Joint Strategic Target Planning Staff JCS Offut AFB Omaha, NB 68113		

DISTRIBUTION LIST

<u>No. of Copies</u>	<u>Organization</u>	<u>No. of Copies</u>	<u>Organization</u>
2	Director US Army BMD Advanced Technology Center ATTN: CRDABH-X CRDABH-S Huntsville, AL 35804	1	Commander US Army Materiel Development and Readiness Command ATTN: DRCDMD-ST 5001 Eisenhower Avenue Alexandria, VA 22333
1	Commander US Army BMD Systems Command ATTN: BDMSC-TFN/N.J. Hurst P.O. Box 1500 Huntsville, AL 35804	1	Commander US Army Armament Research and Development Command ATTN: DRDAR-TDC Dover, NJ 07801
2	Deputy Chief of Staff for Operations and Plans ATTN: Technical Library Director of Chemical & Nuc Operations Department of the Army Washington, DC 20310	3	Commander US Army Armament Research and Development Command ATTN: DRDAR-LCN-F, W. Reiner DRDAR-TSS Dover, NJ 07801
2	Office, Chief of Engineers Department of the Army ATTN: DAEN-MCE-D DAEN-RDM 890 South Pickett Street Alexandria, VA 22304	1	Commander US Army Armament Materiel Readiness Command ATTN: DRSAR-LEP-L Rock Island, IL 61299
3	Commander US Army Engineer Waterways Experiment Station ATTN: Technical Library William Flathau Leo Ingram P.O. Box 631 Vicksburg, MS 39181	1	Director US Army ARRADCOM Benet Weapons Laboratory ATTN: DRDAR-LCB-TL Watervliet, NY 12189
1	Commander US Army Engineering School Ft. Belvoir, VA 22060	1	Commander US Army Aviation Research and Development Command ATTN: DRDAV-E 4300 Goodfellow Boulevard St. Louis, MO 63120
1	US Army MERADCOM ATTN: DRDNE-EM, D. Prink Fort Belvoir, VA 22060	1	Director US Army Air Mobility Research and Development Laboratory Ames Research Center Moffett Field, CA 94035
		2	Commandant US Army Infantry School ATTN: ATSH-CD-CSO-OR Fort Benning, GA 31905

DISTRIBUTION LIST

<u>No. of Copies</u>	<u>Organization</u>	<u>No. of Copies</u>	<u>Organization</u>
1	Commander US Army Communications Rsch and Development Command ATTN: DRSEL-ATDD Fort Monmouth, NJ 07703	4	Commander US Army Natick Research and Development Command ATTN: DRDNA-DT/Dr. D. Sieling DRXNE-UE/A. Johnson A. Murphy W. Crenshaw Natick, MA 01762
3	Commander US Army Electronics Research and Development Command ATTN: DELSD-L DELEW-E, W. S. McAfee DELS-D-EI, J. Roma Fort Monmouth, NJ 07703	1	Commander US Army Tank Automotive Command ATTN: DRSTA-TSL Warren, MI 48090
8	Commander US Army Harry Diamond Labs ATTN: Mr. James Gaul Mr. L. Belliveau Mr. J. Maszaros Mr. J. Gwaltney Mr. F. W. Balicki Mr. Bill Vault Mr. R. J. Bostak Mr. R. K. Warner 2800 Powder Mill Road Adelphi, MD 20783	1	Commander US Army Foreign Science and Technology Center ATTN: Rsch & Concepts Br 220 7th Street, NE Charlottesville, VA 22901
4	Commander US Army Harry Diamond Labs ATTN: DELHD-TA-L DRXDO-TI/002 DRXDO-NP DELHD-RBA/J. Rosado 2800 Powder Mill Road Adelphi, MD 20783	1	Commander US Army Logistics Center ATTN: ATCL-O Mr. Robert Cameron Fort Lee, VA 23801
1	Commander US Army Missile Command ATTN: DRSMI-R Redstone Arsenal, AL 35898	3	Commander US Army Materials and Mechanics Research Center ATTN: Technical Library DRXMR-ER, Joe Prifti Eugene de Luca Watertown, MA 02172
1	Commander US Army Missile Command ATTN: DRSMI-YDL Redstone Arsenal, AL 35898	1	Commander US Army Research Office P.O. Box 12211 Research Triangle Park NC 27709
		4	Commander US Army Nuclear & Chemical Agency ATTN: ACTA-NAW MONA-WE Technical Library MAJ Uecke 7500 Backlick Rd, Bldg. 2073 Springfield, VA 22150

DISTRIBUTION LIST

<u>No. of Copies</u>	<u>Organization</u>	<u>No. of Copies</u>	<u>Organization</u>
1	Commander US Army TRADOC ATTN: ATCD-SA, Mr. O. Wells Fort Monroe, VA 23651	1	Commander Naval Electronic Systems Com ATTN: PME 117-21A Washington, DC 20360
2	Director US Army TRADOC Systems Analysis Activity ATTN: LTC John Hesse ATAA-SL White Sands Missile Range NM 88002	1	Commander Naval Facilities Engineering Command ATTN: Technical Library Washington, DC 20360
1	Commander US Army Combined Arms Combat Developments Activity ATTN: ATCA-CO, Mr. L. C. Pleger Fort Leavenworth, KS 66027	1	Commander Naval Sea Systems Command ATTN: ORD-91313 Library Department of the Navy Washington, DC 20362
1	Commandant Interservice Nuclear Weapons School ATTN: Technical Library Kirtland AFB, NM 87115	1	Commander Naval Weapons Center ATTN: 3431, Tech Lib China Lake CA 93555
1	Chief of Naval Material ATTN: MAT 0323 Department of the Navy Arlington, VA 22217	1	Commander David W. Taylor Naval Ship Research & Development Ctr ATTN: Lib Div, Code 522 Bethesda, MD 20084
2	Chief of Naval Operations ATTN: OP-03EG OP-985P Department of the Navy Washington, DC 20350	1	Commander Naval Surface Weapons Center ATTN: DX-21, Library Br. Dahlgren, VA 22448
1	Chief of Naval Research ATTN: N. Perrone Department of the Navy Washington, DC 20360	2	Commander Naval Surface Weapons Center ATTN: Code W4501/Naval Nuclear Programs Office Code WX21/Tech Lib Silver Spring, MD 20910
1	Strategic Systems Projects Ofc ATTN: NSP-43, Tech Lib Department of the Navy Washington, DC 20360		

DISTRIBUTION LIST

<u>No. of Copies</u>	<u>Organization</u>	<u>No. of Copies</u>	<u>Organization</u>
1	Commander Naval Weapons Evaluation Fac ATTN: Document Control Kirtland Air Force Base Albuquerque, NM 87117	1	Director Lawrence Livermore Lab ATTN: Tech Info Dept L-3 P.O. Box 808 Livermore, CA 94550
1	Commander Naval Research Laboratory ATTN: Code 2027, Tech Lib Washington, DC 20375	1	Director Los Alamos Scientific Lab ATTN: Doc Control for Rpts Lib P.O. Box 1663 Los Alamos NM 87544
1	Superintendent Naval Postgraduate School ATTN: Code 2124, Technical Reports Library Monterey, CA 93940	2	Sandia Laboratories ATTN: Doc Control for 3141 Sandia Rpt Collection L. J. Vortman Albuquerque NM 87115
1	AFSC (Tech Lib) Andrews Air Force Base Washington, DC 20331	1	Sandia Laboratories Livermore Laboratory ATTN: Doc Control for Tech Lib P.O. Box 969 Livermore, CA 94550
1	ADTC (DLODL) Eglin AFB, FL 32542	1	Director National Aeronautics and Space Administration Scientific & Tech Info Fac P.O. Box 8757 Baltimore/Washington International Airport MD 21240
1	AFATL (DLYV) Eglin AFB, FL 32542	1	Aerospace Corporation ATTN: Tech Info Services P.O. Box 92957 Los Angeles, CA 90009
1	RADC (EMTLD/Docu Library) Griffiss AFB, NY 13440	1	Agabian Associates ATTN: M. Agabian 250 North Nash Street El Segundo, CA 90245
1	AFWL/NTES (R. Henny) Kirtland AFB, NM 87115		
1	AFWL/NTE, CPT J. Clifford Kirtland AFB, NM 87115		
1	FTD (NIIS) Wright Patterson AFB Ohio 45433		
1	AFIT (Lib Bldg. 640, Area B) Wright-Patterson AFB Ohio 45433		

DISTRIBUTION LIST

<u>No. of Copies</u>	<u>Organization</u>	<u>No. of Copies</u>	<u>Organization</u>
1	The BDM Corporation ATTN: Richard Hensley P.O. Box 9274 Albuquerque International Albuquerque, NM 87119	1	Lockheed Missiles & Space Co., Inc. ATTN: J. J. Murphy, Dept. 81-11 Bldg. 154 P.O. Box 504 Sunnyvale, CA 94086
1	The Boeing Company ATTN: Aerospace Library P.O. Box 3707 Seattle, WA 98124	1	Martin Marietta Aerospace Orlando Division ATTN: G. Fotieo P.O. Box 5837 Orlando, FL 32805
1	Goodyear Aerospace Corp ATTN: R. M. Brown, Bldg 1 Shelter Engineering Litchfield Park, AZ 85340	2	McDonnell Douglas Astronautics Corporation ATTN: Robert W. Halprin Dr. P. Lewis 5301 Bolsa Avenue Huntington Beach, CA 92647
4	Kaman Avidyne ATTN: Dr. N.P. Hobbs (3 cys) Mr. S. Criscione 83 Second Avenue Northwest Industrial Park Burlington, MA 01830	2	The Mitre Corporation ATTN: Library J. Calligeros, Mail Stop B-150 P.O. Box 208 Bedford, MA 01730
3	Kaman-Nuclear ATTN: Library P. A. Ellis F. H. Shelton 1500 Garden of the Gods Road Colorado Springs, CO 80907	1	Pacific Sierra Research Corp ATTN: Dr. Harold Brode 1456 Cloverfield Boulevard Santa Monica, CA 90404
1	Kaman Sciences Corporation ATTN: Don Sachs Suite 703 2001 Jefferson Davis Highway Arlington, VA 22202	1	Physics International Corp 2700 Merced Street San Leandro CA 94577
1	Kaman-TEMPO ATTN: DASIAC P.O. Drawer QQ Santa Barbara, CA 93102	1	Radkowski Associates ATTN: Peter R. Radkowski P.O. Box 5474 Riverside, CA 92517
1	Kaman-TEMPO ATTN: E. Bryant, Suite UL-1 715 Shamrock Road Bel Air, MD 21014	6	R&D Associates ATTN: Jerry Carpenter J. G. Lewis Technical Library Allan Kuhl (3 cys) P.O. Box 9695 Marina del Rey, CA 90291

DISTRIBUTION LIST

<u>No. of Copies</u>	<u>Organization</u>	<u>No. of Copies</u>	<u>Organization</u>
1	RCA Government Communications Systems 13-5-2 Front & Copper Sts. Camden, NJ 08102	1	California Inst of Tech ATTN: T. J. Ahrens 1201 E. California Blvd. Pasadena, CA 91109
2	Science Applications, Inc. ATTN: Burton S. Chambers John Cockayne P.O. Box 1303 1710 Goodridge Drive McLean, VA 22102	2	Denver Reseach Institute University of Denver ATTN: Mr. J. Wisotski Technical Library P.O. Box 10127 Denver, CO 80210
1	Science Applications, Inc. ATTN: Technical Library P.O. Box 2351 La Jolla, CA 92038	1	IIT Research Institute ATTN: Milton R. Johnson 10 West 35th Street Chicago, IL 60616
1	Systems Science & Software ATTN: C. E. Needham P.O. Box 8243 Albuquerque, NM 87198	1	J. D. Haltiwanger Consulting Services B106a Civil Engineering Bldg. 208 N. Romine Street Urbana, IL 61801
1	Systems Science & Software ATTN: Technical Library P.O. Box 1620 La Jolla, CA 92037	1	Massachusetts Institute of Technology Aeroelastic and Structures Research Laboratory ATTN: Dr. E. A. Witmer Cambridge, MA 02139
1	TRW Systems Group ATTN: Benjamin Sussoltz One Space Park Redondo Beach, CA 92078	2	Southwest Research Institute ATTN: Dr. W. E. Baker A. B. Wenzel 8500 Culebra Road San Antonio, TX 78228
2	Union Carbide Corporation Holifield National Laboratory ATTN: Doc Control for Tech Lib Civil Defense Research Proj P.O. Box X Oak Ridge, TN 37830	1	SRI International ATTN: Dr. G. R. Abrahamson 333 Ravenswood Avenue Menlo Park, CA 94025
1	Weidlinger Assoc. Consulting Engineers ATTN: M. L. Baron 110 East 59th Street New York, NY 10022	1	Stanford University ATTN: Dr. D. Bershader Durand Laboratory Stanford, CA 94305
1	Battelle Memorial Institute ATTN: Technical Library 505 King Avenue Columbus, OH 43201		

DISTRIBUTION LIST

<u>No. of</u> <u>Copies</u>	<u>Organization</u>
1	Washington State University Physics Department ATTN: G. R. Fowles Pullman, WA 99164

Aberdeen Proving Ground

Dir, USAMSAA  
ATTN: DRXSY-D  
DRXSY-MP, H. Cohen  
Cdr, USATECOM  
ATTN: DRSTE-TO-F  
Dir, USACSL  
Bldg. E3516, EA  
ATTN: DRDAR-CLB-PA  
DRDAR-CLN  
DRDAR-CLJ-L